

Article

Natural Hydrogen in Uruguay: Catalog of H₂-Generating Rocks, Prospective Exploration Areas, and Potential Systems

Marcos Sequeira ¹, Ethel Morales ^{1,2}, Isabelle Moretti ^{3,*}, Gerardo Veroslavsky ^{1,2}, Facundo Plenc ^{1,2}, Roberto d'Avila ⁴ and Hector de Santa Ana ⁵

- ¹ PEDECIBA (Programa de Desarrollo de las Ciencias Básicas), Isidoro de María 1614, Montevideo 11800, Uruguay; msequeira@fcien.edu.uy (M.S.); ethel@fcien.edu.uy (E.M.); gerardo@fcien.edu.uy (G.V.); fplenc@fcien.edu.uy (F.P.)
- ² Facultad de Ciencias, UDELAR (Universidad de la República), Iguá 4225, Montevideo 11400, Uruguay
- ³ LFCR, UPPA Rue de l'Université, 64012 Pau, France
- ⁴ Petrobras/E&P/Exploração, EDISEN, Avenida Henrique Valadares, 28, 4o. Andar, Centro, Rio de Janeiro CEP 20.231-030, RJ, Brazil; rdavila@petrobras.com.br
- ⁵ Exploración y Producción, ANCAP (Administración Nacional de Combustibles, Alcohol y Portland), Paysandú s/n y Av. del Libertador, Montevideo 11100, Uruguay; hdesantaana@ancap.com.uy
- * Correspondence: isabelle.moretti@univ-pau.fr

Abstract: The increasing demand for carbon-free energy in recent years has positioned hydrogen as a viable option. However, its current production remains largely dependent on carbon-emitting sources. In this context, natural hydrogen, generated through geological processes in the Earth's subsurface, has emerged as a promising alternative. The present study provides the first national-scale assessment of natural dihydrogen (H₂) potential in Uruguay by developing a catalog of potential H₂-generating rocks, identifying prospective exploration areas, and proposing H₂ systems there. The analysis includes a review of geological and geophysical data from basement rocks and onshore sedimentary basins. Uruguay stands out as a promising region for natural H₂ exploration due to the significant presence of potential H₂-generating rocks in its basement, such as large iron formations (BIFs), radioactive rocks, and basic and ultrabasic rocks. Additionally, the Norte Basin exhibits potential efficient cap rocks, including basalts and dolerites, with geological analogies to the Mali field. Indirect evidence of H₂ in a free gas phase has been observed in the western Norte Basin. This suggests the presence of a potential H₂ system in this area, linked to the Arapey Formation basalts (seal) and Mesozoic sandstones (reservoir). Furthermore, the proposed H₂ system could expand exploration opportunities in northeastern Argentina and southern Brazil, given the potential presence of similar play/tramp.

Keywords: Uruguay; natural hydrogen



Academic Editor: Tadeusz Marek Peryt

Received: 1 January 2025

Revised: 22 January 2025

Accepted: 24 January 2025

Published: 5 February 2025

Citation: Sequeira, M.; Morales, E.; Moretti, I.; Veroslavsky, G.; Plenc, F.; d'Avila, R.; de Santa Ana, H. Natural Hydrogen in Uruguay: Catalog of H₂-Generating Rocks, Prospective Exploration Areas, and Potential Systems. *Geosciences* **2025**, *15*, 54.

<https://doi.org/10.3390/geosciences15020054>

Copyright: © 2025 by the authors. Licensee MDPI, Basel, Switzerland. This article is an open access article distributed under the terms and conditions of the Creative Commons Attribution (CC BY) license (<https://creativecommons.org/licenses/by/4.0/>).

1. Introduction

Climate change, as a global phenomenon driven by anthropogenic activities and greenhouse gas emissions, has become one of the most urgent global challenges of the 21st century. According to the annual climate change report of the Intergovernmental Panel on Climate Change (IPCC), achieving the Paris Agreement's goals to limit the global temperature increase to 1.5 °C requires a rapid and significant reduction in greenhouse gases by 2050 [1]. In this global context, increasing the production of low-carbon energy sources and minimizing the CO₂ emissions from raw material production are essential.

In the last decades, dihydrogen (H₂) has emerged as part of the new energy mix to help carry out decarbonization of the industry and mobility. Its demand has increased

significantly, rising from approximately 40 Mt (million metric tons) in 1990–1995 to 94 Mt in 2021, with expectations to reach 180 Mt in 2030 [2]. H₂ can be generated from multiple sources, including hydrocarbons (with and without carbon capture and sequestration) or water, thanks to the electrolysis process, thus giving it the status of an energy vector. However, today, most of the produced H₂ is generated from fossil sources with CO₂-intensive processes. According to IRENA (n.d.), global H₂ production at the end of 2021 primarily came from natural gas (47%), coal (27%), oil as a by-product (22%), and electrolysis (4%) but mainly from H₂S. The water electrolysis from renewable electricity represents less than 0.5% of the production, evidencing that the current state of H₂ production is still significantly reliant on carbon-emitting processes.

In this global context, Uruguay presents a highly diversified energy matrix with a significant contribution from renewable energy sources, demonstrating the success of having undergone a first energy transition. According to the 2022 energy balance report published by the ministry, the BEN, electricity generation comes from hydroelectric (39%), wind (32%), thermal-biomass (18%), thermal-fossil (9%), and solar (3%) energy sources. Since the electricity sector is largely decarbonized, Uruguay is currently positioned to carry out a second energy transition. In this context, a national “Uruguay’s Roadmap for Green Hydrogen and Derivatives” was released in 2023, supporting a national development for a green hydrogen economy.

However, in recent decades, natural H₂ has emerged as an alternative energy source. It is defined as a “new, clean and low-carbon source of hydrogen that is produced by the Earth, and can migrate and accumulate in geological reservoirs” [3,4]. According to [5], natural H₂ generation may result from different reactions in rocks, such as oxide reduction between Fe²⁺ and H₂O, water radiolysis, and organic late maturation. Its expected commercial costs range between \$1–2/kg or less, which could make it competitive with H₂ from natural gas and coal, which are around \$2/kg and significantly cheaper than green hydrogen, which is announced at around \$ 8/kg but remains much expensive due to the slow start of this industry (Reference [4] and references therein). Therefore, natural H₂ represents one promising new energy source for the 21st century, offering a low-carbon, sustainable, and potentially renewable alternative for hydrocarbons [3,6].

Its natural occurrence has been widely reported. Reference [6] listed 465 sites worldwide, with H₂ appearing as a free, inclusion or dissolved gas in several geological environments, but the list has become larger since the prospection started. Its exploration has been overlooked in the past due to the lack of interest in low-carbon H₂, as well as several erroneous ideas about the impossibility of finding H₂ accumulation, its diffusive character, and fast consumption by microorganisms. All these assumptions were initially incorrect, but exploration remains limited since the mining code still does not include this natural resource in many countries [7].

Currently, H₂ has been exploited in the Bourakebougou field in Mali (West Africa) since 2011 by HYDROMA in the Neo-Proterozoic Taoudeni Basin. They reported a gas composition of mostly pure hydrogen (98%), nitrogen (1%), and methane (1%) [8]. According to [9], the upper reservoirs of the Bourakebougou field are a dynamic hydrogen system that is recharged with natural H₂-rich gas at a production timescale. Other commercial prospectives (currently not exploited) are also reported from geothermal plants in Iceland [10]. The authors reported a total H₂ emissions of 1.16 Kt/year from seven operational geothermal plants with a capacity of approximately 740 MWe between 2019 and 2020. Several natural H₂ occurrences on surface sub-circular depressions (SCDs) or “fairy circles” with specific characteristics in terms of geometry and influence on the vegetation represent an indicator for natural H₂ exploration [11,12]. They have been reported in Russia [13], United States [14], Mali [8], Brazil [15,16], Namibia [12], Australia [17,18],

and Colombia [19], among others. Additionally, natural H₂ exploration worldwide has significantly increased in recent years, with several discoveries reported in the United States, Australia, and France, among others. As a result of this growing and exponential interest in understanding and exploring natural H₂, the number of scientific publications explicitly reporting natural H₂ occurrences has increased significantly over the last few decades [3]. Reserves can not be precisely evaluated since the number of dedicated wells is small, but resources are huge, and they allow for being optimistic about the quantity that could be produced [20,21].

This study presents a first review of potential natural H₂-generating rocks in Uruguay outcropping basement, including their location, geochemical data, and main geological characteristics. Identifying the most promising generating rocks on the surface allows us to infer their presence underlying onshore sedimentary basins, which will be the necessary primary setting for H₂ accumulation. Exploration areas are proposed with a prospective geological analysis (H₂-generating rocks, migration pathways, reservoirs, and cap rocks), providing potential natural H₂ systems for the most promising onshore sedimentary basins. Given the absence of background knowledge on natural H₂ in Uruguay, both from a scientific and governmental perspective, the objective of this study is to conduct the first preliminary assessment of the natural H₂ potential in Uruguay, contributing to its knowledge and establishing guides for its exploration.

2. Uruguay Geological Framework

The Uruguay geological setting is divided into two lithospheric units: a cratonic area (the Rio de la Plata Craton) and an orogenic belt (the Dom Feliciano Belt), along with three main Phanerozoic sedimentary basins (Figure 1). The basement rocks are composed of Precambrian rocks, outcropping in the southern region and in the Rivera and Aceguá “crystalline islands” (northeast Uruguay). Despite different interpretations, three main domains are recognized in the Uruguayan basement from west to east: the Piedra Alta Terrain (PAT), the Nico Pérez Terrain (NPT), and the Dom Feliciano Belt (DFB) (Figure 1A) [22–27].

The PAT, bounded to the east by the Sarandí del Yi Shear Zone (SYSZ) (Figure 1A), represents a juvenile Paleoproterozoic unit related to the Transamazonic orogenic event [24,25]. From south to north, it is composed of three supracrustal metamorphic belts, an extensive granite-gneissic-migmatite area, and late to post-orogenic granitic intrusions [24,28]. In addition, an east–northeast (N70°E) dyke swarm, named Florida Dyke Swarm, intruded the PAT during the Paleoproterozoic [29,30,30,31], among others.

The NPT, located between the SYSZ and the Retamosa Thrust (Figure 1A) [23], is composed of two main structural blocks named Valentines-Rivera Granulitic Complex [24] and Pavas Block [32] (Figure 1A), which were reworked during the Brasiliano–Panafrican Orogenic Cycle [24,33]. It presents high-grade metamorphic Archean to Paleoproterozoic rocks, an extensive anorogenic batholite (Illescas Batholite), and post-orogenic Ediacaran granitic intrusions.

The DFB, located east of the SYSZ and Retamosa Thrust (Figure 1A), represents the results of the Brasiliano–Panafrican Orogenic Cycle (ca. 750–550 Ma) in Uruguay [25]. It extends in a regional northeast direction until the state of Santa Catarina in southern Brazil [34] and comprises basement inliers, supracrustal rocks, granitic intrusions, late Brazilian extensional magmatism, and molassic sequences [23]. Following the regional direction, the DFB is affected by NNE-trending shear zones.

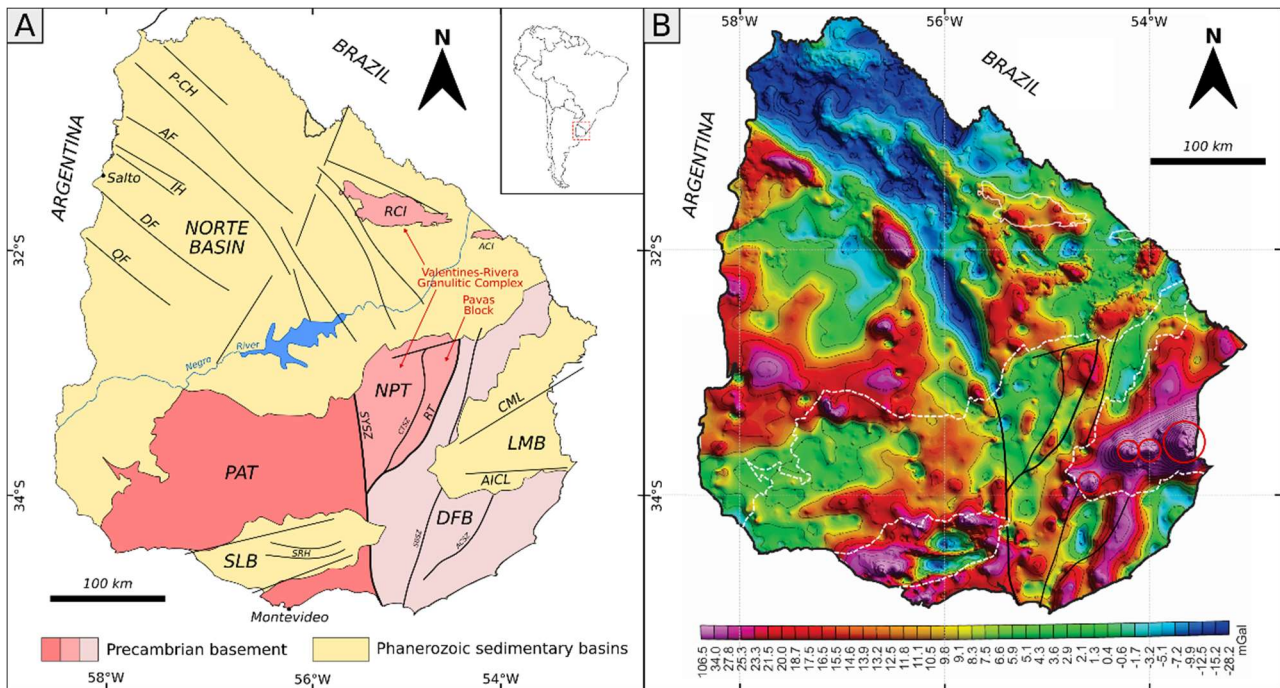


Figure 1. (A) Precambrian basement and its Phanerozoic sedimentary basins (modified from [23,35]). In subfigure the location of Uruguay in South America. (B) Bouguer anomaly map of Uruguay (modified from [36]). Red dotted circles indicate the ring complexes [37] indicated. PAT: Piedra Alta Terrain; NPT: Nico Pérez Terrain; DFB: Dom Feliciano Belt; RCI: Rivera “Crystalline Island”; ACI: Aceguá Crystalline Island; SLB: Santa Lucía Basin; LMB: Laguna Merín Basin; SYSZ: Sarandí del Yi Shear Zone; RT: Retamosa Thrust; SBSZ: Sierra Ballena Shear Zone; CTSZ: Cueva del Tigre Shear Zone; ACSZ: Alférez-Cordillera Shear Zone; AF: Arapey Fault; DF: Daymán Fault; QF: Queguay Fault; IH: Itapebí High; P-CH: Paguero-Cuaró High; SRH: Santa Rosa High; CML: Cebollatí-Merín Lineament; AICL: Aiguá-India Muerta-Chuy Lineament.

Three main sedimentary basins are recognized in onshore Uruguay: the Paleozoic–Mesozoic Norte Basin (NB), the Mesozoic Santa Lucía (SLB), and the Laguna Merín (LMB) basins in the south (Figure 1A). The NB represents the Uruguayan portion of the larger intracratonic Paraná Basin (Brazil) and Chaco-Paraná Basin (Argentina). Located in northern Uruguay, it comprises Paleozoic to Mesozoic sedimentary rocks and basaltic flows related to the western Gondwana fragmentation and evolution. Basin infill is divided into four mega-sequences bounded by regional unconformities: (a) Devonian: shallow marine and transitional sedimentary rocks outcropping in the south NB region [38]; (b) late-Carboniferous to Permian: glacial deposits that transition to fluvial and aeolian deposits at top [39]; (c) Jurassic–Cretaceous: continental, fluvial and aeolian sedimentary rocks, and volcanic rocks up to 1000 m thickness of basalt flows [39,40]; (d) Upper Cretaceous: fluvial continental deposits restricted to the western NB region [41]. The maximum sedimentary thickness was recorded in the Salto and Belén wells (2206 and 2336 m, respectively). However, the targets of both exploratory wells were anticline structural highs [42]. Based on geophysical information, [35] infer a potential maximum basin thickness of ~3500–3700 m in western NB lows through the Arapey–Dayman corridor. Basin infill is controlled by two main structural features inherited from basement compartmentalization. The NNE–SSW structures are associated with regional discontinuities that were reactivated during the Late Paleozoic by dextral transcurrent movements, while the NW–SE structures were reactivated during the Late Permian and primarily the Mesozoic, controlling the Cretaceous volcanic emplacement and structural lows and highs [43] (Figure 1).

In southern Uruguay, two pull-apart intracratonic basins are present through the Santa Lucía-Aiguá-Merín N70° structural lineament [44–46]. The SLB was formed through ENE crustal weakness in the PAT [24,47] (Figure 1A). It comprises a sedimentary infill of basaltic flows at the base and continental Mesozoic fluvial, aeolian, and lacustrine deposits, with a thin Cenozoic sedimentary cover. Its internal configuration presents two main sub-basins to the north and south of the E–W Santa Rosa High (Figure 1). The LMB, in southeastern Uruguay, has an ENE structural configuration bounded to the north by the Cebollatí-Merín Lineament (N50°) and to the south by the Aiguá-India Muerta-Chuy Lineament (N85°) (Figure 1) [44,48]. It is mainly composed of igneous Jurassic–Cretaceous rocks and a Cretaceous to Cenozoic sedimentary cover. Maximum depths were recorded in the Puerto Gómez N°502 well with a total depth of 1360 m [49]. Based on the results from magnetotelluric surveys, Reference [49] indicates a maximum basin thickness infill of 2500 m.

3. Material and Methods

Firstly, a potential H₂-generating rock catalog was performed, following the generating rock classification described by [5], which defines four types of rocks based on their affinity for hydrogen generation processes: (i) H₂_GR1: basic and ultrabasic rocks of mantle/oceanic affinity (e.g., peridotites, gabbros, and basalts), which generate natural H₂ through their hydrothermal alteration; (ii) H₂_GR2: iron-bearing rocks (banded iron formations (BIFs), intrusive rocks (e.g., biotite-rich granites)) with the potential to generate natural H₂ through redox processes during aqueous alteration; (iii) H₂_GR3: radioactive continental rocks, which generate natural H₂ through radiolysis processes involving H₂O; (iv) H₂_GR4: organic-rich rocks (coal, shaly coals, and shales) that generate natural H₂ at high temperatures regardless of H₂O presence. The potential for natural H₂ generation is related to critical parameters such as Fe²⁺/Fe^{tot} for H₂_GR1 and H₂_GR2, the content of radioactive elements (U, Th, and K) for H₂_GR3 and the Total Organic Carbon (TOC) for H₂_GR4. Due to the absence of Fe-speciation data on potential natural H₂-generating rocks in Uruguay, the total content of FeO or Fe₂O₃ is provided as a preliminary proxy. For generating rock abbreviations references, see the summarized catalog in Table 1. This catalog details the location, geochemical data, and main geological characteristics of each H₂-generating rock. The data were collected from a literature review and from airborne geophysical data for radioactive elements (U, Th, and K) content. The geophysical data were acquired during 2014–2015 by the Geological Survey of Uruguay (DINAMIGE-MIEM), covering close to 90% of Uruguayan basement rocks (excluding the Rivera “Crystalline Island”) [23].

Based on a review of geological and geophysical data from onshore sedimentary basins, an integral analysis of prospective areas and potential H₂ systems was performed, defining the generation, accumulation, and trapping processes. The models were conducted following the analogy to petroleum systems already exposed in the literature for natural H₂ exploration [6,17,19,50–53], among others. These areas will represent the most favorable locations for large-scale natural H₂ accumulation for future exploration. A review of logging data from old exploration wells in the most promising areas was also conducted.

Table 1. Summarized potential natural H₂-generating rocks catalog.

<i>H₂_GR1</i>	<i>Geological unit</i>	<i>ID</i>	<i>Domain</i>	<i>Fe content</i>				<i>References</i>
Serpentinites	Paso del Dragón Fm.	S1	DFB	2.55–5.17%; 10.25–17.68% (Fe₂O₃)				[34,54]
	Ojosmín Complex	S2	TPA	9.7% (Tremolite); 16.5% (Gabbro) (Fe₂O₃)				[28]
	Tapes Complex	S3	DFB	7.56%; 15.88% (Fe₂O₃)				[55,56]
	Arroyo Grande Fm.	S4	TPA	<i>n.d.</i>				-
Gabbros	Guaycurú Complex	G1	TPA	8.0% (FeO); 3.2% (Fe₂O₃)				[57,58]
	Isla Mala Suite	G2	TPA	8.5 ± 1%; 7.71–9.84% (Fe₂O₃) (Rospide)				[58,59]
	Lascano alkaline serie	G3	LMB	12.39–13.08% (Fe₂O₃)				[37]
	Coronilla	G4	LMB	11.38–15.97% (Fe₂O₃)				[37]
	Carbonera	G5	LMB	9.86–11.19% (Fe₂O₃)				[37]
Mafic Dyke Swarms	Florida	DS1	TPA	8.21–12.67%; 7.93–13.25% (FeO)				[22,60]
	Nico Pérez-Zapican	DS2	TPA/NPT/DFB	<i>n.d.</i>				-
<i>H₂_GR2</i>	<i>Geological unit</i>	<i>ID</i>	<i>Domain</i>	<i>Fe content</i>				<i>References</i>
BIFs	Valentines Fm.	I1	NPT	33–46%; 40.83–52.25% (Fe)				[61,62]
	Vicahedero Fm.	I2	NPT	<i>n.d.</i>				[63]
	Cebollatí/Las Tetas Complex	I3	DFB	<i>n.d.</i>				-
	Arroyo del Soldado Group	I4	DFB	35.45–40.06% (Fe₂O₃) (Yerbal Fm.)				[64]
	Marco de los Reyes Fm.	I5	DFB	55 ± 6% (Fe₂O₃)				[28]
	Manguera Azul Fm.	I6	DFB	<i>n.d.</i>				-
	Paso Severino Fm.	I7	PAT	<i>n.d.</i>				-
<i>H₂_GR3</i>	<i>Geological unit</i>	<i>ID</i>	<i>Domain</i>	<i>Radiometric (Cps)</i>	<i>K (%)</i>	<i>Th (ppm)</i>	<i>U (ppm)</i>	<i>References</i>
Granite Intrusions	Illescas batholith	<i>R1</i>	NPT	12,100	5.1	132	28	[23]
	Florencia (Aiguá batholith)	<i>R2</i>	DFB	3900	4.4	34	7	[23]
	Los Cerrillos (Aiguá batholith)	<i>R3</i>	DFB	3480	4.1	28	6	[23]
	José Ignacio	<i>R4</i>	DFB	2800	4.2	21	2	[23]
	Santa Lucía batholith	<i>R5</i>	DFB	4557	5.2	48	7	[23]
	Polanco	<i>R6</i>	DFB	4245	4.1	36	7	[23]
	Cerro de las Cuentas	<i>R7</i>	NPT	4345	4.9	38	6	[23]
	Cuchilla Dionisio batholith	<i>R8</i>	DFB	3680	4.1	33	4	[23]
	Correzuelo	<i>R9</i>	NPT	3320	4.7	27	3	[23]
	Sierra de Ánimas Complex	<i>R10</i>	DFB	3320	4.6	22	5	[23]
	Sierra de Ríos Fm.	<i>R11</i>	DFB	3560	4.2	33	5	[23]
<i>H₂_GR4</i>	<i>Geological unit</i>	<i>ID</i>	<i>Domain</i>	<i>TOC (%)</i>				<i>References</i>
Coals	Tres Islas Fm.	<i>O1</i>	NB	<i>n.d.</i>				-
Oil shales	Mangrullo Fm.	<i>O2</i>	NB	8.93; 12.5				[65,66]
Gas shales	Cordobés Fm.	<i>O3</i>	NB	3.6				[65]

4. Results: Potential Natural H₂-Generating Rocks

4.1. Basic and Ultrabasic Rocks from Mantellic/Oceanic Affinity (H₂_GR1)

Basic and ultrabasic rocks, serpentinites, gabbros, and mafic dyke swarms, are widely present in Uruguay, mainly in the PAT and LMB.

4.1.1. Serpentinites

The presence of serpentinites in Uruguay is restricted to the Paso del Dragón Complex and the Tapes Complex in the DFB, and the Ojosmín Complex and the Arroyo Grande Formation in the PAT.

The Paso del Dragón Complex (S1; hereafter refer to Figure 2 and Table 1), located at the northern extreme of the DFB, is an allochthonous Neoproterozoic fragment composed of two lithodemic units: La Micaela Schist and Cerro La Tuna serpentinites [34]. According to the authors, the Cerro La Tuna serpentinites comprise deformed and lower greenschist metamorphic facies serpentinites, tremolite schists/granofels, talc, and chlorite schists. These mafic and ultramafic rocks exhibit a trend ranging from N20°E to E–W within the Paso del Dragón Complex. Several authors, including [67], consider the Paso del Dragón Complex as an ophiolite relict, and regional correlations link this complex to the Chameis Gate Ophiolitic Complex (Marmora Terrain of the Gariiep Belt) in South Africa [54] or with the Arroio Grande Ophiolitic Complex in Rio Grande do Sul, Brazil [68]. Despite different interpretations, the possible ophiolitic genesis of the Paso del Dragón Complex highlights its potential as a natural H₂ generating rock. However, its outcropping area is restricted, and superficial rocks present high alteration (already serpentinized), so its potential interest has to be considered in its subsurface extent. Reference [56] presents geochemical data for the Cerro La Tuna amphibolites, with Fe₂O₃ values ranging from 10.25% to 17.68% (wt.%), while others present values between 2.55% to 5.17% (wt.%).

In the central PAT, an assemblage of tremolites, gabbros, and a meta volcano-sedimentary succession grouped in the Ojosmín Complex (S2) (probably Paleoproterozoic) is described by [28], outcropping as a tectonic fenster. Geochemical data for tremolites and gabbros indicate MORB and depleted mantle affinity, suggesting to the authors that the Ojosmín Complex could be related to an ophiolitic relict. Fe₂O₃ values for the tremolites and gabbros are 9.7% and 16.5% (wt.%), respectively, based on the average of only two samples. Despite the authors highlighting its potential interest as an ophiolitic relict, no additional studies were conducted subsequently.

The Tapes Complex (S3) is a Mesoproterozoic volcano-sedimentary succession characterized by low-grade metamorphism (greenschist facies). It is composed of chlorite schist, metawackes, serpentinites, tremolitites, cherts, and limestones. With a regional NE structural trending orientation, the Tapes Complex outcrops in two main areas: the Mariscal (N30°E) and Zapicán (N70°E) belts (see review in [56]). According to petrographic analysis, serpentinites mineralogy presents serpentine, talc, tremolite, chlorite, dolomite, and magnetite. Reported serpentines geochemical data present Fe₂O₃ values of 7.56% (wt.%) [56] and 15.88% (wt.%) [55].

The Arroyo Grande Formation (S4) is a lower to middle-grade metamorphic volcano-sedimentary succession located in the northern PAT with a regional NNE–E structural trend. It is composed of Paleoproterozoic [69] serpentinites, rhyolites, metabasalts, andesites, and variable sedimentary facies from conglomerates to mudstones [28]. No geochemical data are presented for the serpentinites until date.

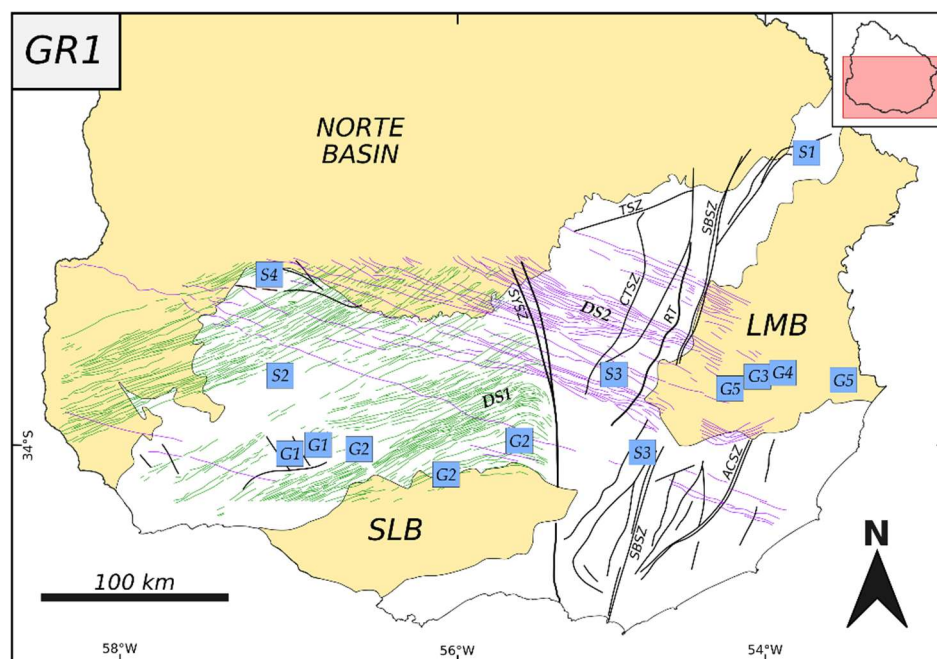


Figure 2. Serpentinites, gabbros, and mafic dyke swarm locations, i.e., H₂_GR1, in southern Uruguay (modified from [23,31]). SLB: Santa Lucía Basin; LMB: Laguna Merín Basin; SYSZ: Sarandí del Yí Shear Zone; RT: Retamosa Thrust; SBSZ: Sierra Ballena Shear Zone; CTSZ: Cueva del Tigre Shear Zone; ACSZ: Alférez-Cordillera Shear Zone; TSZ: Tupambaé Shear Zone.

4.1.2. Gabbros

The presence of basic igneous intrusions is mostly restricted to the PAT in southwest Uruguay and to the LMB, where several gabbros are mapped (Figure 2).

The Guaycurú Complex (G1), located in south-central region of the PAT, presents several Paleoproterozoic gabbros, gabbro-norites, and norites intrusions of tholeiitic affinity [28]. The presence of olivine in the different intrusion mineralogy has been reported by several authors [70], highlighting a 5–10% olivine content in La Mandarinina gabbro [57]. Additionally, [70] report FeO and Fe₂O₃ content values of 8.0% and 3.2% (wt.%), respectively, based on a single sample from the Mahoma gabbro. The gravimetric results presented by [71] suggest an average depth of 2000 m for the intrusion in the same area.

Reference [60] compiled several Paleoproterozoic intrusions in the PAT and referred to them as the Isla Mala Suite (G2). The authors included the Rospide gabbro, the Carreta Quemada hornblende gabbro, and Reboledo (gabbros and hornblendites). For a detailed mineralogical description, refer to the review by [55]. Regarding the Rospide gabbro, [58] presented geochemical results of Fe₂O₃ with values around 8.5 ± 1% (wt.%), while [59] indicates Fe₂O₃ values ranging between 7.71% to 9.84% (wt.%) (from four samples).

Other individual gabbros are reported in the PAT (e.g., San Carlos gabbro and Maríncho Complex, among others). However, due to the absence of detailed petrographic and geochemical studies, they are not considered in the current catalog.

In southeastern Uruguay, Reference [38] described several early Cretaceous gabbro intrusions within four ring complexes related to the intrusive magmatic evolution of the LMB (Figures 1B and 2). They reported a series of gabbros within the Puerto Gómez Formation [72], specifically the Lascano alkaline series (G3), Coronilla (G4), and Carboneras Units (G5). The gabbros present the highest densities (up to 2.00 g/cc) and Fe₂O₃ content within the intrusive complex, with values ranging from 9.86% to 15.97% (wt.%).

Additionally, the authors propose that gravity anomalies in the area (Figure 1B) are the result of the shallow emplacement of these gabbro dykes, sills, and plugs, which are genetically related to a possible more voluminous underlying intrusion at depths of up to 5 km.

4.1.3. Mafic Dyke Swarms

Based on recent airborne magnetic data, Reference [32] characterized two main regional dyke swarms in the Uruguay basement, named Florida and Nico Pérez-Zapican (Figure 2). According to Euler deconvolution results, the authors estimated root depths ranging from 0 to 500 m, suggesting surface to shallow dyke emplacements.

The Florida Dyke Swarm (DS1) is restricted to the PAT and represents a 250 km long and 200 km wide swarm of ENE dyke intrusions with dips around 90° to 60° (to the north). According to field data from [60], individual intrusions present a 30 m width and an average length of 1000 m. Outcropping dolerites dykes from the Florida Dyke Swarm were characterized by [27], which described rocks of andesitic composition with high titanium content (group A) and andesitic-basaltic rocks of low titanium content (group B). Reference [23] presents geochemical results from 14 samples, with FeO values mainly ranging between 8.21% to 12.67% (wt.%) (except for one sample with 1.54% FeO content). Additionally, [60] differentiated the same groups described by [27] and presented geochemical data of FeO with values ranging from 10.95% to 13.25% (wt.%) (group A) and 7.93% to 9.07% (wt.%) (group B), from 28 samples taken from 16 individual dykes.

The Nico Pérez-Zapican Dyke Swarm (DS2) crosscuts the Uruguayan basement, mostly in the NPT. It has a general ESE orientation (N100–110°E) and covers an area of 350 km long and 150 km wide. Mesozoic tholeiitic basalt dykes with the same trend were described by [73] in a limited area within the region of the Nico Pérez-Zapican Dyke Swarm, as identified by [31]. No geochemical data are reported.

Despite being individual intrusive rocks, the high spatial frequency of these regional and voluminous mafic dyke swarms in Uruguay suggests they may be considered as an additional potential source of natural H₂. The mapped area extent of the dyke swarms observed in Figure 2 reflects the limits of the airborne survey coverage.

4.2. Iron-Bearing Rocks (H₂_GR2)

Banded Iron Formation

Paleoproterozoic and Neoproterozoic BIFs have been described in the basement rocks of Uruguay. The most voluminous iron resources in Uruguay are within the Valentines Formation in central NPT and Vichadero Formation in the Rivera “Crystalline Island” (NPT), both part of the Valentines-Rivera Granulitic Complex [24] (Figures 1 and 3). According to the authors, this complex may continue in southeastern Brazil (~100–130 km from the Uruguayan frontier) in the Taquarembó Block.

The Valentines Formation (I1; hereafter refer to Figure 3 and Table 1) is an Arquean to Paleoproterozoic high-metamorphic (granulitic facies) and deformed iron-rich formation located in central NPT [74,75]. With an outcropping area of ~850 km², the Valentines Formation represents one of the highest magnetic anomalous units (up to 3185 nT in its internal subdomain) in the Uruguayan basement rocks [23] (Figure 3B). It is composed of gneisses, granites, pyroxenites, and magnetite-augitic quartzites, locally referred to as “Valentinesite” due to its unique mineral composition not previously described in the literature. The Valentinesites are banded iron formations with a maximum Fe₂O₃ between 28 and 35%, and a mineral assemblage of quartz (40%), magnetite (33%), and aegirine-augite (25%) [61]. Based on the results from around 800 drill cores and surface geochemical samples, a minimum Fe content of 33%, a maximum of 46%, and an average of 38.5% (wt.%)

were reported. Additionally, geochemical results from drill cores in the Valentines and Las Palmas areas reported Fe concentrations ranging from 40.83% to 52.25% (wt.%) (in terms of total Fe_2O_3) [62]. Geochemical signatures suggest that iron-rich rock protolith from the Valentines Formation were deposited in suboxic to anoxic waters with high-temperature hydrothermal fluids [62].

The Valentines Formation represents the largest iron-rich deposit in Uruguay. Exploration campaigns in the area were conducted between 1950 and 1960, and more recently in the 2010s, when detailed mapping and drilling quantified the mineral resources [76]. According to information from the recent exploration company, a total resource of 764 Mt of iron was measured.

The Vichadero Formation (I2) is an Early Paleoproterozoic [77] high-metamorphic (granulitic facies) and deformed iron-rich formation outcropping in the Rivera “Crystalline Island” basement horst, within the NB [76]. According to the authors, the Vichadero Formation comprises BIFs, manganese iron formations, quartzite, forsterite marble, calcisilicate granofels, clinopyroxene granofels, tremolite granofels, and mafic metavolcanic rocks. Based on petrographic and geochemical results, four types of BIFs and Mn-rich formations were classified. Group 1 represents BIFs composed of centimeter-sized quartz, magnetite, and hematite minerals, while group 2 presents BIFs with the same mineralogical content as group 1 with manganese silicates, including pyroxene, pyroxenoid, and amphibole. Both groups present SiO_2 and Fe_2O_3 values > 90% (wt.%). Group 3 consists mostly of garnet-bearing rocks, and group 4 comprises massive iron-manganese rocks. Protolith genetic interpretations suggest a chemical sediment enrichment in a chert and carbonate shelf succession for the BIFs.

Chronological and geological similarities between the Valentines and Vichadero Formation indicate a coeval formation [76]. According to the authors, iron resources from both BIFs represent more than 600 Mt with values around 28% Fe (wt.%), thereby representing the main iron-bearing natural H_2 potential generating rocks of Uruguay.

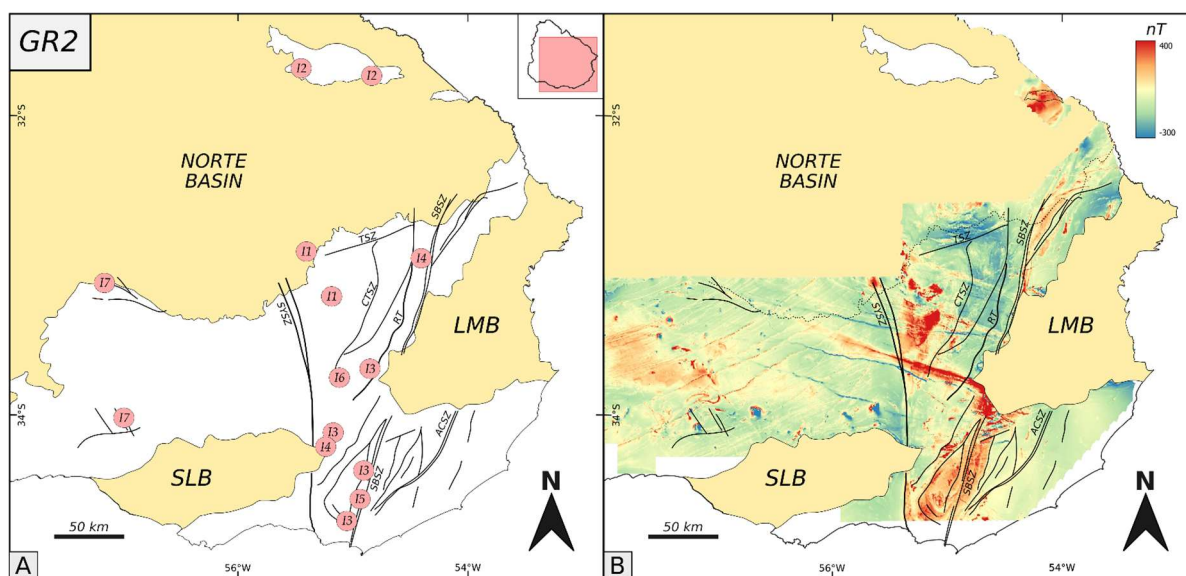


Figure 3. (A): BIFs locations (modified from [76]). (B): Anomalous magnetic field reduced to the pole map (modified from [23]). SLB: Santa Lucía Basin; LMB: Laguna Merín Basin; SYSZ: Sarandí del Yí Shear Zone; RT: Retamosa Thrust; SBSZ: Sierra Ballena Shear Zone; CTSZ: Cueva del Tigre Shear Zone; ACSZ: Alferéz-Cordillera Shear Zone; TSZ: Tupambaé Shear Zone.

In western DFB, the presence of Paleoproterozoic BIFs is described in the Cebollatí Complex (I3) [78], also known as the Las Tetás Complex [79]. The Archean to Paleoproterozoic

zoic succession presents highly deformed and medium metamorphic grade (amphibolite facies) metaquartzite, micaschist, metaconglomerate, and marble. The authors indicate the presence of BIFs in the Arroyo Malo Formation, and in the Cerro del Diamante Formation (25 m thickness of BIFs), which the authors grouped into the Cebollatí Group. According to [76], the presence of BIFs in the Cebollatí Group is scattered.

Neoproterozoic BIFs are present in western DFB, in the Arroyo del Soldado Group (I4) [80]. It represents an Ediacaran marine shelf succession, in which the presence of BIFs is reported in the Cerro Espuelitas and Yermal formations. The Cerro Espuelitas Formation presents an upper succession of up to 110 m of BIFs and cherts. The BIFs are alternating bands of magnetite to hematite with a maximum Fe_2O_3 content of 35% (wt.%) and average values of 21% (based on 21 samples). The formations were later redefined as a succession of shales and cherts, with iron-rich rocks at the top, indicating that no BIFs were documented. The Yermal Formation represents a 1500 m succession of interbedded mudstones, sandstones, carbonates, cherts, and BIFs. BIFs from the Yermal Formation reach a maximum thickness of 50 m and, according to [81], are composed of 24% magnetite/hematite. Total Fe_2O_3 content ranges between 35.45% to 40.06% (wt.%).

Reference [71] indicates the presence of metamorphic BIFs in amphibolite facies (taconite) within the Marco de los Reyes Formation in the Carapé Group (I5) or Zanja del Tigre Formation. According to the authors, the formation is a Neoproterozoic succession of taconites (metamorphic BIFs), limestones, micaschists, quartzites, amphibolites, and gneisses. Average values of $55 \pm 6\%$ of Fe_2O_3 (wt.%) content were reported in the taconites. However, its surface presence is not well developed.

Additional scattered BIF occurrences are also recorded in the Manguera Azul Formation (I6) (Paleoproterozoic carbonatic succession) [82] with millimetric levels of quartz and hematite in a lower dolomitic-siliciclastic member, and in the PAT in the Paso Severino Formation (I7) (Paleoproterozoic sedimentary succession). However, their spatial dimensions are small, and no geochemical data for the BIFs are presented at date.

4.3. Radioactive Rocks (H_2_GR3)

Radioactive rocks in the Uruguayan basement can be identified by the radiometric (total counts) and potassium (K), thorium (Th), and uranium (U) signature content maps presented by [23]. According to the authors, the radiogenic values of these elements were mapped in the upper 0.5 m of the surface. As shown in Figure 4, the highest radiometric values are predominantly related to intrusive rocks in the NPT and DFB. No anomalous values are recognized in the PAT. Although the authors conduct a detailed analysis of the radiometric content in the Valentines Formation, the Illescas Batholith, and the Sierra de Ánimas Complex, the present catalog also includes a brief description of several Neoproterozoic intrusions in both domains, which exhibit high radiometric values, indicating their potential as radioactive rocks. The Valentines Formation was previously characterized by its iron-rich content; hence, no further information is provided below. For K (%), Th (ppm), and U (ppm) contents, see Table 1.

The Illescas Batholith (R1; hereafter refer to Figure 4, Table 1), located in the western NPT within the Valentines-Rivera Complex, presents the major radiometric anomalous values in the NPT [23]. It represents the largest granitic intrusion with an outcropping area up to 750 km², crosscut on its western flank by the SYSZ (Figure 4). Geochronological data indicate a Statherian crystallization age (1768 ± 11 Ma in [83]). It comprises mostly granites with rapakivi texture, representing an anorogenic intraplate magmatism event. According to [23], high values of radioactivity (up to 12,100 total cps) were verified in the B2 subdomain defined by the authors, in which two anomalous peaks are observed. The

south peak presents K, Th, and contents of 3.7%, 132 ppm, and 28 ppm, while the north peak presents values of 2.7%, 117 ppm, and 12 ppm, respectively.

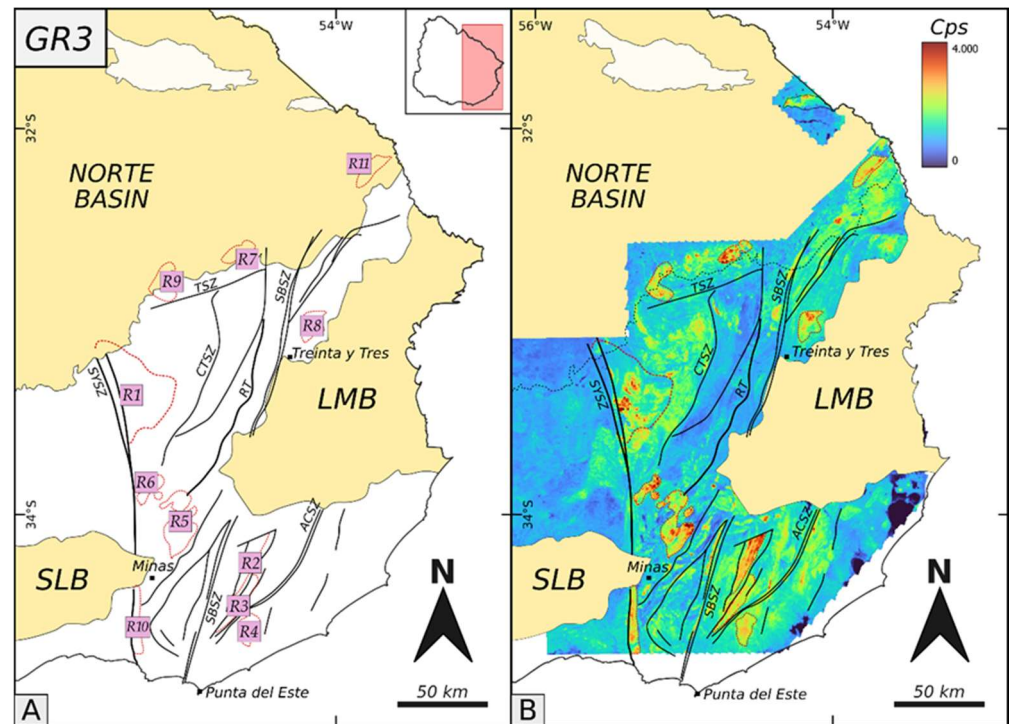


Figure 4. (A): Radioactive intrusive rocks in NPT and DFB with the position of the known H₂_GR3. (B): Radiometric map of total counts (counts per second) of the NPT and DFB (data from [23]). SLB: Santa Lucía Basin; LMB: Laguna Merín Basin; SYSZ: Sarandí del Yi Shear Zone; RT: Retamosa Thrust; SBSZ: Sierra Ballena Shear Zone; CTSZ: Cueva del Tigre Shear Zone; ACSZ: Alferez-Cordillera Shear Zone; TSZ: Tupambaé Shear Zone.

In the DFB, several high radiometric values are related to Brasiliano orogenic event intrusive rocks. A series of calco-alkaline granite intrusions, grouped into the Aiguá batholith [32], are reported between the Sierra Ballena Shear Zone and Alferez-Cordillera Shear Zone (R2 and R3). Figure 4B suggests that the highest total radiometric values up to 3900 and 3480 (total cps) within the batholite correspond to the Florencia (R2) and Los Cerrillos granites (R3), respectively, described by [84] in a detailed study of the area. The intrusions consist of isotropic (Florencia) to deformed (Los Cerrillos) equigranular granites with quartz, potassic feldspar, and biotite.

Southeast of the Alferez-Cordillera Shear Zone, high radiometric values (up to 2800 total cps) are also observed in the Ediacaran José Ignacio granite (R4) [85]. The intrusion outcrops in an area, extend ~270 km² and presents inequigranular granitic lithologies compounds of quartz, feldspar, and biotite [84].

North of the city of Minas, several circular and sharp contact granitic intrusions exhibit high radiometric values (Figure 4). Reference [82] named these individual granite intrusions as Marmarajá, Arroyo del Soldado, Barriga Negra, and Polanco. The first three are usually grouped into the Puntas del Santa Lucía batholith (R5). The batholith comprises several intrusions of granites, granodiorites, monzogranites, and syenites with equigranular and isotropic textures, reaching radiometric values up to 4557 (total cps). Reference [83] reported a crystallization age of 633 ± 8 Ma in a monzogranite. The Polanco granite (R6), northwest of the Santa Lucía batholith, presents maximum radiometric values of 4245 (total cps).

Additional high radiometric values are observed in the northern NPT close to the NB boundary and in northern DFB, close to the Treinta y Tres city (Figure 4). These values are

related to Brasiliano granitic intrusion and are named by [85] as the Cerro de las Cuentas (R7), Treinta y Tres (R8) (DFB), and Cerrezuelo (R9) (NPT) granites. Reference [84] mapped the Treinta y Tres as Cuchilla Dionisio granite (R8), describing a porphyric and isotropic granite with high contents of biotite, in which a crystallization age of 577 ± 2 Ma is reported. According to Figure 4, radiometric values up to 4345, 3680, and 3320 (total cps) are reported for the Cerro de las Cuentas, Arroyo Malo, and Cerrezuelo granitic intrusions, respectively.

Volcanic intrusions with high radiometric values are also reported in the Sierra de Ánimas Complex (R10) and Sierra de Ríos Formation (R11). The first presents radiometric counts up to 3320 total cps and high amounts of K, Th, and U [23]. The complex exhibits an N–S trend with a length of 50 km and a width of 5–10 km, parallel to the SYSZ. Lithologies comprise syenites, microsyenites, trachytes, granophyres, rhyolites, and basalts, representing an Ediacaran magmatism event [86]. The Sierra de Ríos Formation reached radiometric values up to 3560 (total cps). The formation is a compound of rhyolites and ignimbrites with an age of 575 ± 14 Ma.

4.4. Organic-Rich Rocks (H_2 _GR4)

In Uruguay, the current O&G exploration is taking place offshore, but organic-rich rocks are also mostly outcropping in the northeast NB within the Permian Tres Islas (coals) and Mangrullo (oil shales) formations and in the Devonian Cordobés Formation (gas shales) [65].

The Tres Islas Formation (O1; hereafter referred to as Figure 5, Table 1) is an Early Permian deltaic sedimentary succession present in the north to northeast NB, with a maximum thickness of 160 m, as reported in the El Águila well [39]. According to [39], it is divided into two members. The lower member comprises arkosic to subarkosic sandstones, conglomeratic sandstones, and conglomerates restricted to the southeast basin boundary. The upper member is compound of fine quartzose to micaceous sandstones, with black shales, coals, and argillaceous limestones associated, suggesting the transition of deltaic deposits to prodelta and marine shelf. The presence of coals in Uruguay is restricted to the Tres Islas Formation, with the highest potential found south of the city of Melo (Figure 5) [39]. Despite the fact that the presence of coal levels has been recognized in several exploration wells, its exploration potential is limited by its small thickness. In Brazil, its correlative formation (Rio Bonito Formation) hosts the vast majority of coal deposits in the country. The Candiota coal deposit is located 50 km northwest of the Cerro Largo department, in the Uruguayan frontier (Figure 5). Natural H_2 discoveries were recently reported in four wells in the southern Paraná Basin in Brazil (Rio Grande do Sul and Santa Catarina states) [53]. The authors indicate that the highest values (up to 8.79% of H_2) are geologically linked to the maturation of coals and shales layers of the Rio Bonito, Taciba, and Ponta Grossa formations.

Another potential organic-rich rock in Uruguay are the oil shales from the Mangrullo Formation (O2). This formation is an Early Permian sedimentary succession developed under restricted underwater conditions, with a maximum thickness of up to 35 m in the northeast NB boundary, correlated to the Iratí Formation in southern Brazil (Figure 5). It comprises organic-rich shales, mudstones, and carbonates [39,87]. According to the authors, the Mangrullo Formation is the only proven fossil fuel in Uruguay, with two main oil shales levels with a maximum TOC of 12.5%. More recently, [66] exposed the results from a source through rock quality analyses of two wells samples in which 8.93% of TOC and 2.02 (S1) and 46.92 (S2) mg/g from the Rock Eval analyses are presented. The Tmax and vitrinite reflectance values were 399 ± 3 °C and 0.61%. The authors define the Mangrullo Formation shales as a good to excellent source rock, which is immature, but entering the oil window near the outcropping area (Figure 5). According to the H_2 occurrences already mentioned

in southern Brazil, the organic-rich shales from the Irati Formation could also contribute to natural H₂ generation in the Paraná Basin. The most plausible areas are where the organic-rich rocks are intruded by magmatic sills due to their maturation increase.

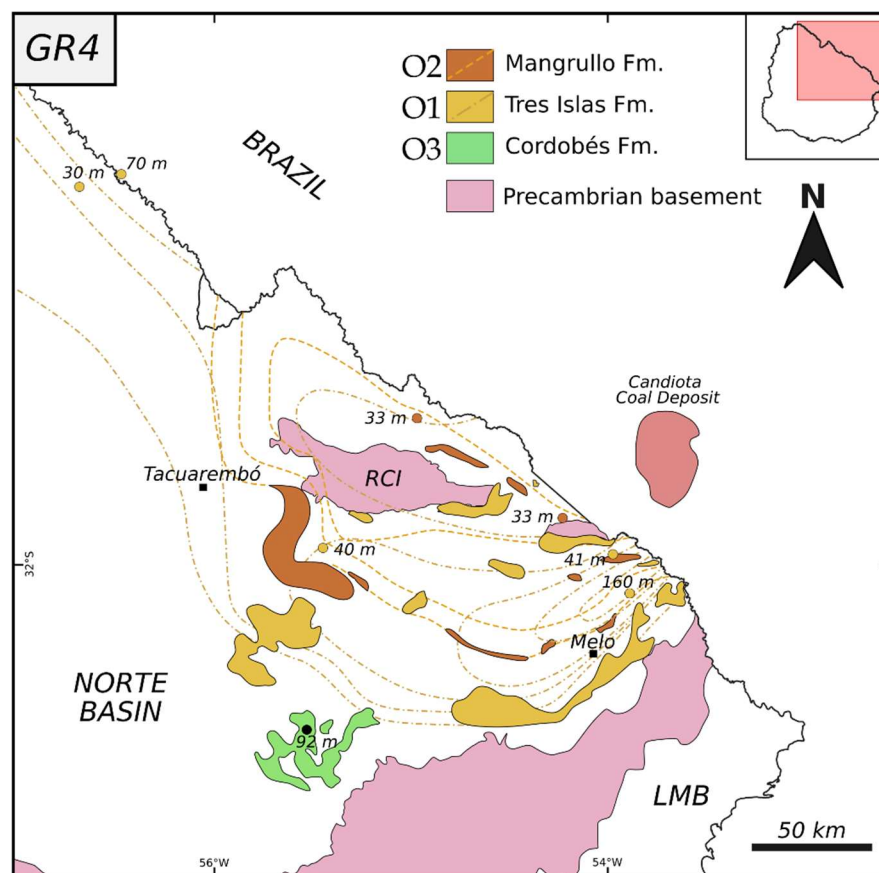


Figure 5. Organic-rich rocks outcropping locations in northeast NB (data from de [39]) depicting the Candiota coal deposit in southern Brazil (data from [53]). LMB: Laguna Merín Basin; RCI: Rivera “Crystalline Island”.

The Cordobes Formation (O3) (its equivalent, Ponta Grossa Formation in Brazil) is the third potential organic-rich rock in Uruguay. It comprises homogenous Early Devonian, shallow marine shales with maximum thicknesses of 92 m (La Paloma well) located in the southern NB boundary (Figure 5). It presents TOC values of around 3.6% [65].

Although the occurrence of potential organic-rich rocks is primarily restricted to northeast Uruguay, their presence in western NB is also inferred from structural and geophysical data [35,43,88]. According to the authors, the occurrence of pre-Carboniferous rocks could be restricted to structural lows within the Arapey-Dayman corridor at depths of approximately 3500 m (Figure 1). Assuming the presence of potential Devonian organic-rich rocks at these depths, a higher maturation level is very likely.

5. Prospective Areas Analysis

Four regional prospective areas with differential geological characteristics for natural H₂ exploration are presented (Figure 6). Each region was defined by its particular basement rocks, sedimentary cover, and geophysical characteristics. While the LMB is presented individually, the NB was divided into three potential areas (NB1, NB2, and NB3). The eastern part of the NB (DFB domain) is considered to have no potential for natural H₂ exploration due to the lack of sedimentary infill. This integral analysis summarizes the natural H₂

system models for each region, depicting their potential H₂-generating rocks, reservoirs, traps, and migration pathways. A brief description of each region is presented below.

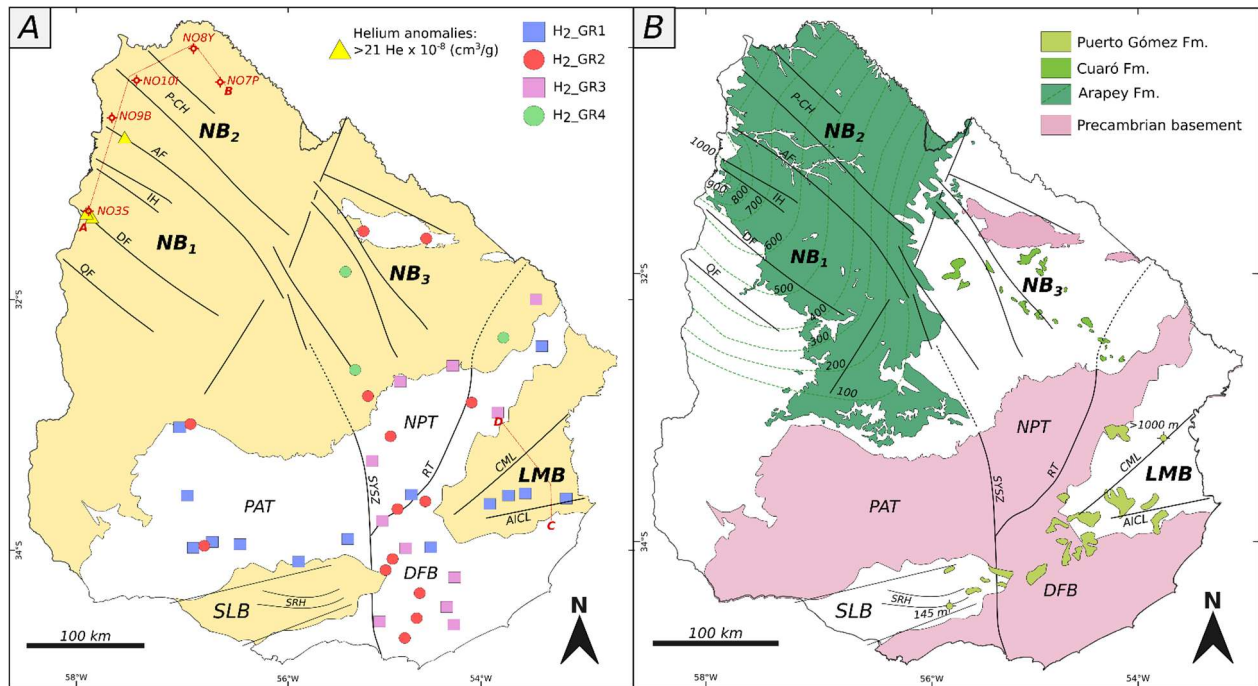


Figure 6. (A): Prospective onshore sedimentary basin areas, depicting the potential natural H₂-generating rocks location. (B): Basalt flows formations outcropping areal extent, depicting the isopach map (m) of the Arapey Formation, and the maximum thickness in basin wells for the Puerto Gómez Formation. AF: Arapey Fault; DF: Daymán Fault; QF: Queguay Fault; IH: Itapebí High; P-CH: Paguero-Cuaró High; CML: Cebollatí-Merín Lineament; AICL: Aiguá-India Muerta-Chuy Lineament; SYSZ: Sarandí del Yi Shear Zone; RT: Retamosa Thrust.

5.1. Western Norte Basin

The NB1 area is restricted to the south of the Arapey Fault, overlying the PAT. According to recent studies, the SYSZ (PAT eastern limit) continuing beneath the NB follows the Bouguer anomaly map lineament (Figures 1B and 6), aligning in the northwest with the orientation of the Arapey Fault [89]. Higher values of up to 25–30 mGal are observed in the NB1 relative to the outcropping PAT, matching the B2 and B3 structural domains with a mean crustal thickness of 37.5 and 36 km, respectively, as defined by [36]. Based on the H₂-generating rock catalog, gabbros and mafic dyke swarms are expected to be the potential H₂-generating rocks for the area. The serpentinization of gabbros has already been proposed as responsible for natural H₂ generation in Kansas, United States [90]. According to [91], serpentinization processes are most active at temperatures between 200 and 300 °C. Based on average geothermal gradient values in the area [92,93], the most productive serpentinization processes are expected to occur at depths of more than 7 km in the area. However, other authors showed that low-temperature serpentinization also took place, as currently in Oman [94], very likely due to the oxidation of other iron oxides [95] or iron carbonates [96]. In addition, H₂ generation, through radiolysis processes, must be considered due to the presence of helium anomalies in the dissolved gases of the confined Guarani Aquifer System [97]. The study reported maximum values ranging from 21 to 97 × 10⁻⁸ cm³/g in five wells located along the Dayman and Arapey Faults in the NB1 area (Figure 6A), suggesting radioactive decay processes.

As expressed in the catalog, additional H₂ generation could be related to the late maturation of pre-Carboniferous organic-rich rocks preserved on structural lows (Figure 7).

The maximum sedimentary cover is reached in the northern region, where more than 2500–3000 m depths are expected between the Arapey and Daymán Faults, and more than 4000 m to the west in Argentina [88]. It is not deep enough to generate H₂ with a normal gradient; at least 200 °C is necessary [98,99], but local higher maturation could be present in this volcano-sedimentary basin. The presence of deep-seated faults, which intersect basement rocks is observed from the seismic sections in the area [35]. The Guaraní Aquifer System, hosted by Mesozoic sandstones and trapped by the Arapey Formation (Figure 7), presents evidence of mixing with deeper waters in this area, suggesting that deep-seated faults may act as fluid migration pathways.

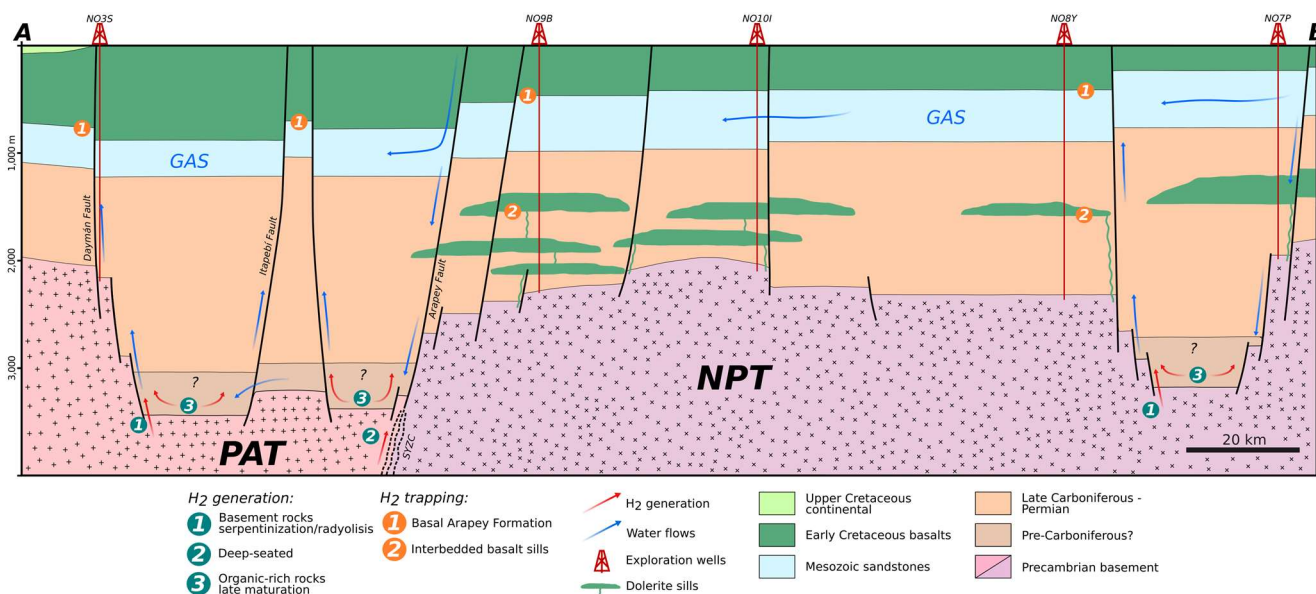


Figure 7. Geological cross section of the western NB (see location in Figure 6), depicting potential natural H₂ generation, migration pathways, and trapping (section modified from [35]). PAT: Piedra Alta Terrain; NPT: Nico Pérez Terrain; GAS: Guaraní Aquifer System.

The NB2 area is located north of the Arapey Fault, overlying the western NPT. Its eastern limit is defined by a strong change in gravity values (between 0 to −30 mGal) (Figures 1B and 6) and by the different potential reservoirs and cap rocks compared to the NB3 area. It presents a maximum mean crustal thickness of 38.5 km [36]. Potential H₂-generating rocks are related to those described in the catalog for the NPT (BIFs and radioactive rocks). The maximum basin sedimentary infill is reached in its northwestern area, with values up to 2500 m, but higher depths are inferred at structural lows (Figure 7).

The main potential reservoirs for NB1 and NB2 are represented by the sandstones of the Mesozoic Tacuarembó and Itacumbú, and Early and Late Permian Tres Islas and Buena Vista formations. Depths must be considered for natural H₂ solubility in the presence of aquifers, and will be discussed later in the natural H₂ system section. We propose that the cap rocks would be the basalt flows of the Arapey Formation (equivalent to the Serra Geral Formation) and genetically related dolerite sills interbedded in the Late Carboniferous–Permian mega-sequence (Figures 6B and 7). The Arapey Formation [72], represents more than 40,000 km² of the Lower Cretaceous tholeiitic basalt flows related to the Paraná-Etendeka province’s effusive lavas (Figure 6B). Maximum thickness values of 955 and 460 m are recorded in the NO3S (NB1) and NO9B (NB2), respectively (Figure 7). The philonian rocks related to NB magmatic evolution are grouped within the Cuaró Formation [85]. It comprises the Cretaceous tholeiitic sills and dykes mainly developed in a regional NW-SE trend (Figure 6B). Several dolerite sills are reported in exploration wells in NB2, interbedded within the Late Carboniferous–Permian mega-sequence, suggesting

deeper and potentially localized cap rocks (Figure 7). According to [100], the thickness of the dolerites in the Bourakebougou field represents a key control on H₂ accumulation and trapping. Subsurface efficient dolerites' thickness ranges between 100 and 150 m, while below 20 m thick their trapping efficiency is non-effective. Figure 7 illustrates dolerites sills with thicknesses of more than 100 m drilled by wells.

5.2. Eastern Norte Basin

The NB3 represents the eastern part of the NB overlying the NPT. Higher gravity values are observed compared to the NB2 (0 to 20 mGal) and a mean crustal thickness of 36.5 km [36]. The presence of outcropping BIFs between the geologically linked Valentines and Vichadero formations suggests that these rocks may also be present in the southern area of the Rivera "Crystalline Island", in the NB3 basement (Figure 6). As documented in the catalog, the iron content in both BIFs represents the major volumes in Uruguay. Additionally, the highest radioactive values are present in the NPT outcropping area (Illescas batholith), suggesting potentially similar H₂-generating rocks for the NB3. In this area, basin depths range from 200 to 600 m from east to west [101]. Recent studies on redox processes in BIFs provide evidence that natural H₂ could be generated at very shallow depths (<50 °C) through aqueous alteration during surface weathering processes [102]. In addition, batch reactor experiments on magnetite minerals (previously considered a by-product of H₂ generation) interacting with anoxic waters have been shown to generate H₂ at low temperatures [95]. The occurrence of shallower basement rocks in regions predominantly characterized by BIFs indicates a highly promising exploration area.

The potential targeted reservoirs will be shallower than those of the northwest NB. Early Permian Tres Islas Formation sandstones are the only expected reservoir in this area. Cap rocks will relate to cretaceous dolerite sills, which outcrop in the area (Figure 6B), but may also be interbedded deeper within the proposed reservoirs. The Bourakebougou field presents shallow reservoirs at depths of 100 m within dolerites traps as well [8,9]. The presence of water in this area is associated with the San Gregorio and Tres Islas formation aquifers, which can be located at the base of the basin in this region and, therefore, reacting with basement rocks.

5.3. Laguna Merín Basin

H₂-generating rocks related to the DFB (radioactive, gabbros) may be present in the LMB basement. This region exhibits a positive Bouguer anomaly of up to ~100 mGal in the subsurface and a mean crustal thickness of 33.5 km [36], aligned with a magnetic anomaly of up to ~1200 nT [37]. This feature has an ellipsoidal shape measuring 80 km by 40 km, oriented structurally from east to northeast [37]. This anomaly suggests the presence of an ultramafic rock body located at depths greater than 4 km beneath the LMB, as indicated by magnetotelluric profiles of the area, which reported a deep, conductive, intrusive body in the basement [48]. Additionally, high-resolution airborne gravity and magnetic data revealed several anomalous circular features (20–30 km diameter) related to volcanic intrusive rocks' ring complexes [37] (Figure 1B). These features correspond to the same area where the gabbros previously reported in the catalog for the LMB were described. Genetic interpretations suggest mafic intrusions akin to the Bushveld- or Trumpsberg-type [103] or caldera structures associated with mafic intrusive complexes [37]. The presence of geophysical anomalies and potential ultramafic rocks in the subsurface suggest that the serpentinization of such rocks could potentially generate significant volumes of natural H₂. However, there is a lack of hydrogeological information regarding potential deep aquifers. According to magnetotelluric data [48], the basin is bounded by deep-seated

normal faults rooted in the basement. The southern fault could connect the subsurface potential ultramafic rocks to potential shallow reservoirs.

Magnetotelluric profiles evidence the presence of conductive levels up to 500 m thickness at the lower half of the basin infill [48]. The authors correlate these conductive values ($<25 \Omega \cdot \text{m}$) with possible inter-trap sandstones or highly altered basalts, suggesting potential reservoirs, covered by a thick volume (non-conductive) of volcanic rocks (Figure 8). No deepest potential reservoirs are expected at the basin base, beneath the basalts. In LMB, Early Cretaceous basalt flows are grouped into the Puerto Gómez Formation [72], where more than 1000 m thickness are reached in the Puerto Gómez N°502 well (Figure 6B). These volcanic rocks have to be considered as primary cap rocks for the basin.

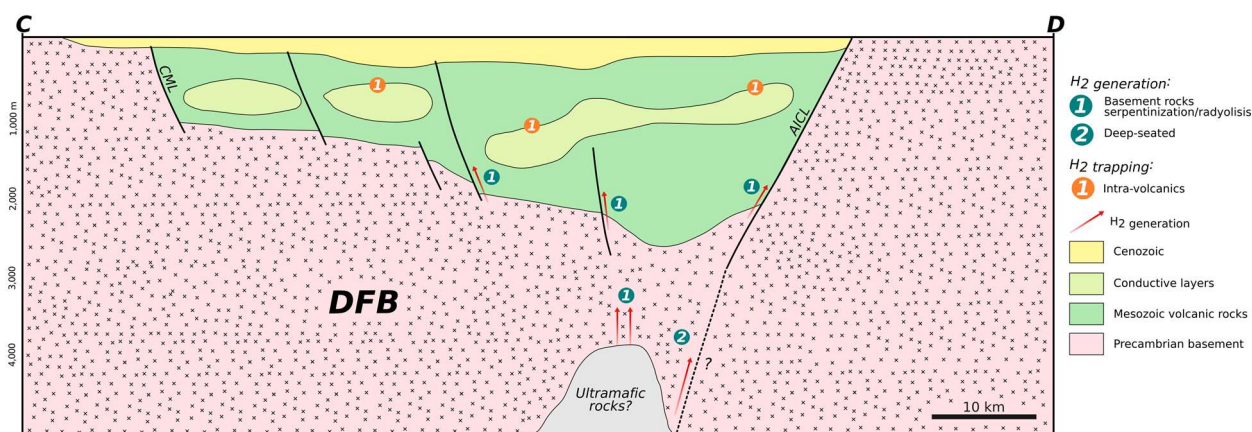


Figure 8. Geological cross section of the LMB (see location in Figure 6), depicting potential natural H_2 generation, migration pathways, and trapping (modified from [35]). DFB: Dom Feliciano Belt; CML: Cebollati-Merín Lineament; AICL: Aiguá-India Muerta-Chuy Lineament.

6. Discussion: An Analogous Natural H_2 System from the Malian Field in Uruguay?

The Bourakebouougou field in Mali represents the only commercially exploited natural H_2 system worldwide to date, operating at a very local scale. Recent studies have focused on the reservoir and seal characteristics [8,9,100]. It presents the first shallow carbonate-free gas H_2 reservoir at about 100 m depth, along with two additional deeper free gas H_2 sandstone reservoirs. The shallower reservoir appears to cover an 8 km regional area extent. The brine spot of the seismic suggests that the accumulation is not continuous, but rather that it consists of various small shallow free gas accumulations. In addition, dissolved H_2 has also been reported in two other sandstone reservoirs below an 800 m depth, where wells have been drilled down to 2 km, suggesting that the aquifer is saturated in H_2 . Dolerite sills have been there identified as efficient seals.

Neutron logging is the primary tool for identifying potential natural H_2 reservoirs when simple gas logging data are absent [9]. Neutron logging reflects the hydrogen atom content in rocks and fluids, with higher values indicating high clay content or a gas effect in rocks. In the carbonate upper reservoir, the authors observed a clear offset between the neutron and density logging, suggesting that it is a preliminary indirect indicator of natural H_2 presence.

We conducted a review of neutron logging borehole data from deep exploration wells drilled in the 1980s in western NB, Uruguay. Neutron logging values from the NO8Y well in the NB2 area (Figure 6) show an anomalous increase between 421 and 433 m depths with a clear offset with the density log, not observed at deeper depths (Figure 9A). Similarly to observations in Mali, this offset could suggest the hypothesis of the presence of a gas phase containing H_2 . This interval, ranging up to 10 m thick, is identified in a medium to coarse

quartzose sandstone to conglomerate, with rounded grains and good sorting, within the upper Tacuarembó Formation. Gamma-ray values in this interval are very low, measuring up to 20 gAPI below a depth of 422 m (Figure 9A), suggesting no clay content.

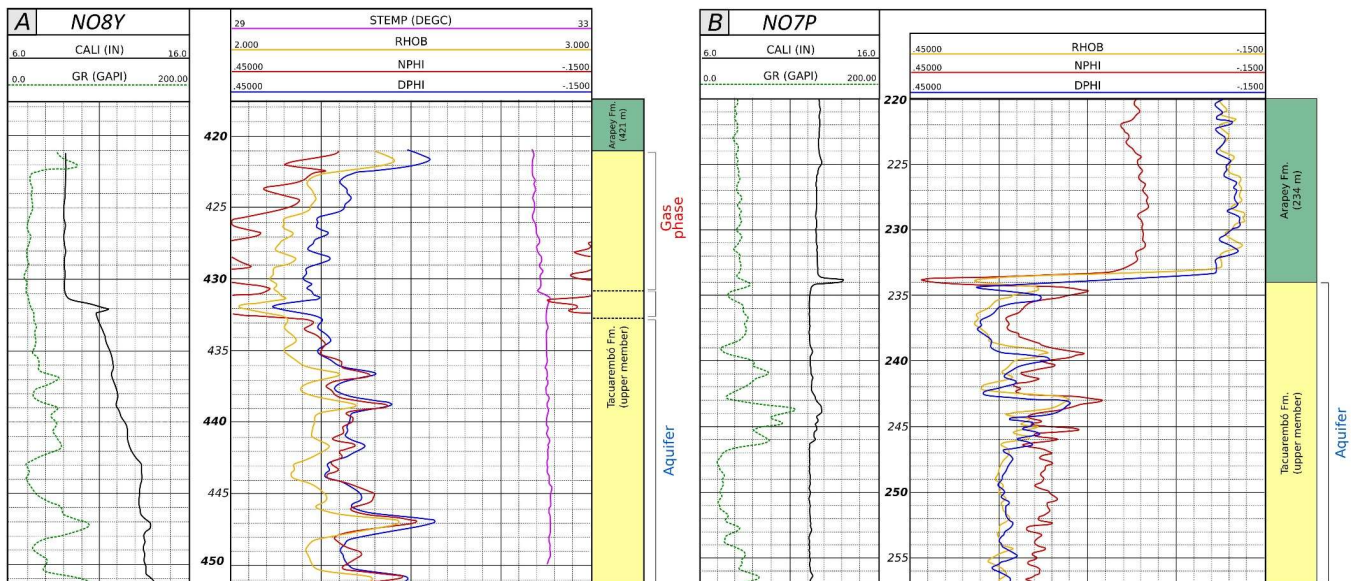


Figure 9. (A): NO8Y (Yacaré) well logging borehole data. (B): NO7P (Pelado) well logging borehole data (modified from [104]). See locations in Figure 6A. CALI: caliper; GR: natural gamma-ray log; STEMP: temperature log; RHOB: bulk density log; NPHI: neutron log; DPHI: density log.

The upper Tacuarembó Formation is bounded to the top by the Arapey Formation basalts that reach 421 m in thickness in the NO8Y well, probably acting as a seal for this potential natural H₂ reservoir. An abrupt change in temperature logging at 431 m is likely associated with the presence of the aquifer (Figure 9A). The interval between 431 and 433 may represent a transition phase between the aquifer and the upper free gas zone. It is noteworthy that no hydrocarbon gas content was detected at this interval during continuous mud logging, and while chromatography analysis was conducted during drilling.

Only one additional well (NO7P) has neutron logging data in the same stratigraphic interval (at the base of the Arapey Formation basalts). The well is located 37 km southeast of the previously described well (Figure 6). The NO7P well did not report any increase in neutron values below the contact between the Arapey and upper Tacuarembó formations (Figure 9B). These data support the hypothesis that the neutron anomaly in the NO8Y well could be related to a potential natural H₂ reservoir with a limited areal extent.

Indirect borehole data allows us to propose a natural H₂ system in western NB, related to the upper Tacuarembó Formation sandstones as reservoirs, trapped by the basalts of the Arapey Formation (Figure 7), representing the most promising efficient seal. Potentially lower dolerite sills, with more than 100 m thickness, may act as an additional cap rock for lower reservoirs. Free gas H₂ window depths in the presence of aquifers must be considered according to experimental data [105] or modeling [106] on the solubility of H₂ in water and brine. As observed in the Mali case, increasing quantities of H₂ are expected to be dissolved at greatest depths. Events related to the proposed potential hydrogen system for NB are summarized in Figure 10. The presence of helium anomalies in the same stratigraphic interval, as indirect borehole data suggest a possible co-association of both gases, as observed in other locations [107]. A gas vector (or mixture) is required for the movement and migration of helium in the subsurface, such as H₂, N₂, CO₂, or hydrocarbon gases (Brown, 2010).

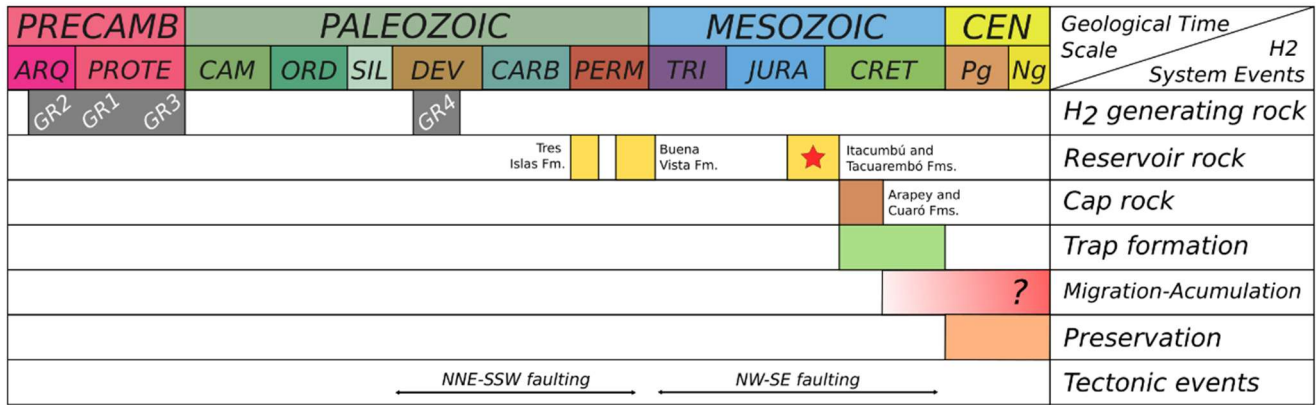


Figure 10. Natural H₂ system events chart proposed for NB. The red star indicates a neutron anomaly.

The proposed hydrogen system and plays may also be present in northeastern Argentina (Chaco-Paraná Basin), and southern Brazil (Paraná Basin). It is noteworthy that the only commercial hydrocarbon discovery in the Paraná Basin, the Barra Bonita gas field (southern Brazil), is found in Carboniferous-Permian sandstones, which are trapped by dolerite sills [108,109].

7. Conclusions

Uruguay exhibits significant potential for natural hydrogen exploration. Based on the results of the present study, several conclusions regarding the prospectivity of natural H₂ in Uruguay can be drawn:

1. The presence of outcropping rocks with the potential for natural H₂ generation has been identified and cataloged, allowing for the inference of expected H₂ generation underlying onshore sedimentary basins at optimal conditions of depth, temperature, and H₂O presence.
2. The western NB is identified as a key area for exploration due to the presence of major basement depths, potential sandstone reservoirs, basalts, and related dolerite cap rocks, deep-seated faults, and inferred deep aquifers.
3. Notable potential is observed in the eastern NB, associated with H₂ generation from the oxidation of potential BIFs and potential trapping by dolerites, as well as in the LMB, due to gravimetric anomalies. However, further studies and data acquisition are required in both areas for further exploration.
4. A hydrogen system is proposed for western NB, related to upper Tacuarembó Formation sandstones as reservoirs, trapped by the Arapey Formation basalts as cap rocks. Additional lower reservoirs with dolerites as cap rocks are proposed. The proposed plays/tramps for western NB present geological analogies of the Mali field, and the only proven hydrocarbon commercial discovery in the Paraná Basin.

The present study represents the first national-scale assessment of natural H₂ potential in Uruguay, providing an example of analysis for other regions. Despite the fact that scientific knowledge on natural H₂ generation, migration, and trapping processes is still in its “infancy”, this assessment of the most prolific exploration areas in Uruguay will support increased scientific and industrial interest. Further studies by the present research group will focus on surface gas seep detection and monitoring across deep-seated faults and sub-circular depressions, along with total gas geochemistry and isotopic signature analysis, in the most promising exploration areas.

Author Contributions: The conceptualization, investigation, and methodology of this paper was developed by M.S. Validation and supervision were carried out by E.M. and I.M. The original draft was prepared by M.S. and the review and editing were carried out by E.M., I.M. and G.V. Visualization was handled by G.V., F.P., R.d. and H.d.S.A. All authors have read and agreed to the published version of the manuscript.

Funding: The research that led to the results presented in this publication was funded by the Agencia Nacional de Investigación e Innovación (ANII) under the code POS_NAC_2023_1_177882.

Data Availability Statement: All data are within the cited bibliography.

Acknowledgments: Authors would like to thanks to ANCAP for providing the well data.

Conflicts of Interest: The authors declare no conflicts of interest.

References

1. Calvin, K.; Dasgupta, D.; Krinner, G.; Mukherji, A.; Thorne, P.W.; Trisos, C.; Romero, J.; Aldunce, P.; Barrett, K.; Blanco, G.; et al. *IPCC, 2023: Climate Change 2023: Synthesis Report. Contribution of Working Groups I, II and III to the Sixth Assessment Report of the Intergovernmental Panel on Climate Change*; Core Writing Team, Lee, H., Romero, J., Eds.; Intergovernmental Panel on Climate Change (IPCC): Geneva, Switzerland, 2023.
2. IEA. Global Hydrogen Review 2021. Public Report. Available online: <https://www.iea.org/reports/global-hydrogen-review-2021> (accessed on 22 January 2025).
3. Gaucher, E.C.; Moretti, I.; Péliissier, N.; Burrige, G.; Gonthier, N. The Place of Natural Hydrogen in the Energy Transition: A Position Paper. *Eur. Geol.* **2023**, *5*–9. [[CrossRef](#)]
4. Blay-Roger, R.; Bach, W.; Bobadilla, L.F.; Reina, T.R.; Odriozola, J.A.; Amils, R.; Blay, V. Natural Hydrogen in the Energy Transition: Fundamentals, Promise, and Enigmas. *Renew. Sustain. Energy Rev.* **2024**, *189*, 113888. [[CrossRef](#)]
5. Wang, L.; Jin, Z.; Chen, X.; Su, Y.; Huang, X. The Origin and Occurrence of Natural Hydrogen. *Energies* **2023**, *16*, 2400. [[CrossRef](#)]
6. Zgonnik, V. The Occurrence and Geoscience of Natural Hydrogen: A Comprehensive Review. *Earth-Sci. Rev.* **2020**, *203*, 103140. [[CrossRef](#)]
7. Hand, E. Hidden Hydrogen. *Science* **2023**, *379*, 630–636. [[CrossRef](#)] [[PubMed](#)]
8. Prinzhofer, A.; Cissé, C.S.T.; Diallo, A.B. Discovery of a Large Accumulation of Natural Hydrogen in Bourakebougou (Mali). *Int. J. Hydrogen Energy* **2018**, *43*, 19315–19326. [[CrossRef](#)]
9. Maiga, O.; Deville, E.; Laval, J.; Prinzhofer, A.; Diallo, A.B. Characterization of the Spontaneously Recharging Natural Hydrogen Reservoirs of Bourakebougou in Mali. *Sci. Rep.* **2023**, *13*, 11876. [[CrossRef](#)] [[PubMed](#)]
10. Combaudon, V.; Moretti, I.; Kleine, B.L.; Stefánsson, A. Hydrogen Emissions from Hydrothermal Fields in Iceland and Comparison with the Mid-Atlantic Ridge. *Int. J. Hydrogen Energy* **2022**, *47*, 10217–10227. [[CrossRef](#)]
11. Moretti, I.; Brouilly, E.; Loiseau, K.; Prinzhofer, A.; Deville, E. Hydrogen Emanations in Intracratonic Areas: New Guide Lines for Early Exploration Basin Screening. *Geosciences* **2021**, *11*, 145. [[CrossRef](#)]
12. Moretti, I.; Geymond, U.; Pasquet, G.; Aimar, L.; Rabaute, A. Natural Hydrogen Emanations in Namibia: Field Acquisition and Vegetation Indexes from Multispectral Satellite Image Analysis. *Int. J. Hydrogen Energy* **2022**, *47*, 35588–35607. [[CrossRef](#)]
13. Larin, N.; Zgonnik, V.; Rodina, S.; Deville, E.; Prinzhofer, A.; Larin, V.N. Natural Molecular Hydrogen Seepage Associated with Surficial, Rounded Depressions on the European Craton in Russia. *Nat. Resour. Res.* **2015**, *24*, 369–383. [[CrossRef](#)]
14. Zgonnik, V.; Beaumont, V.; Deville, E.; Larin, N.; Pillot, D.; Farrell, K.M. Evidence for Natural Molecular Hydrogen Seepage Associated with Carolina Bays (Surficial, Ovoid Depressions on the Atlantic Coastal Plain, Province of the USA). *Prog. Earth Planet. Sci.* **2015**, *2*, 31. [[CrossRef](#)]
15. Prinzhofer, A.; Moretti, I.; Françolin, J.; Pacheco, C.; D’Agostino, A.; Werly, J.; Rupin, F. Natural Hydrogen Continuous Emission from Sedimentary Basins: The Example of a Brazilian H₂-Emitting Structure. *Int. J. Hydrogen Energy* **2019**, *44*, 5676–5685. [[CrossRef](#)]
16. Moretti, I.; Prinzhofer, A.; Françolin, J.; Pacheco, C.; Rosanne, M.; Rupin, F.; Mertens, J. Long-Term Monitoring of Natural Hydrogen Superficial Emissions in a Brazilian Cratonic Environment. Sporadic Large Pulses versus Daily Periodic Emissions. *Int. J. Hydrogen Energy* **2021**, *46*, 3615–3628. [[CrossRef](#)]
17. Frery, E.; Langhi, L.; Maison, M.; Moretti, I. Natural Hydrogen Seeps Identified in the North Perth Basin, Western Australia. *Int. J. Hydrogen Energy* **2021**, *46*, 31158–31173. [[CrossRef](#)]
18. Mainson, M.; Heath, C.; Pejčić, B.; Frery, E. Sensing Hydrogen Seeps in the Subsurface for Natural Hydrogen Exploration. *Appl. Sci.* **2022**, *12*, 6383. [[CrossRef](#)]
19. Ramirez, A.C.; Penagos, F.G.; Rodriguez, G.; Moretti, I. Natural H₂ Emissions in Colombian Ophiolites: First Findings. *Geosciences* **2023**, *13*, 358. [[CrossRef](#)]

20. Ellis, G.S.; Gelman, S.E. Model Predictions of Global Geologic Hydrogen Resources. *Sci. Adv.* **2024**, *10*, eado0955. [[CrossRef](#)]
21. Lévy, D.; Roche, V.; Pasquet, G.; Combaudon, V.; Geymond, U.; Loiseau, K.; Moretti, I. Natural H₂ Exploration: Tools and Workflows to Characterize a Play. *Sci. Technol. Energ. Transition* **2023**, *78*, 27. [[CrossRef](#)]
22. Bossi, J.; Campal, N.; Civetta, L.; Demarchi, G.; Girardi, V.A.V.; Mazzucchelli, M.; Negrini, L.; Rivalenti, G.; Fragoso Cesar, A.R.S.; Sinigoi, S.; et al. Early Proterozoic Dike Swarms from Western Uruguay: Geochemistry, Sr Nd Isotopes and Petrogenesis. *Chem. Geol.* **1993**, *106*, 263–277. [[CrossRef](#)]
23. Bettucci, L.S.; Loureiro, J.; Demarco, P.N. Airborne Geophysical Characterization of Uruguayan Basement. *J. South Am. Earth Sci.* **2021**, *108*, 103206. [[CrossRef](#)]
24. Oyhantçabal, P.; Siegesmund, S.; Wemmer, K. The Río de La Plata Craton: A Review of Units, Boundaries, Ages and Isotopic Signature. *Int. J. Earth Sci.* **2011**, *100*, 201–220. [[CrossRef](#)]
25. Bettucci, L.S.; Peel, E.; Masquelin, H. Neoproterozoic Tectonic Synthesis of Uruguay. *Int. Geol. Rev.* **2010**, *52*, 51–78. [[CrossRef](#)]
26. Cesar, A.R.S.F. O Cráton Do Río de La Plata e o Cinturão Dom Feliciano No Escudo Uruguaio-Sul-Riograndense. *Anais* **1980**, *5*, 2879–2892.
27. Bossi, J.; Campal, N. Magmatismo y Tectónica Transcurrente Durante El Paleozoico Inferior En Uruguay. In *Paleozoico Inferior de Iberoamérica*; Gutiérrez-Marco, J.G., Saavedra, J., Rábano, I., Eds.; Universidad de Extremadura: Badajoz, Spain, 1992; pp. 343–356.
28. Bossi, J.; Piñeyro, D. *Carta Geológica Del Uruguay a Escala 1/500,000, Versión Digital 2.0*; Facultad de Agronomía: Montevideo, Uruguay, 2014.
29. Bossi, J.; Campal, N. *Granitos Negros Filonianos Del Uruguay: Resultados de Las Investigaciones*; CIID-Facultad de Agronomía, Universidad de la República: Montevideo, Uruguay, 1991; pp. 1–71.
30. Halls, H.C.; Campal, N.; Davis, D.W.; Bossi, J. Magnetic Studies and U–Pb Geochronology of the Uruguayan Dyke Swarm, Rio de La Plata Craton, Uruguay: Paleomagnetic and Economic Implications. *J. South Am. Earth Sci.* **2001**, *14*, 349–361. [[CrossRef](#)]
31. Demarco, P.N.; Masquelin, H.; Prezzi, C.; Aifa, T.; Muzio, R.; Loureiro, J.; Peel, E.; Campal, N.; Bettucci, L.S. Aeromagnetic Patterns in Southern Uruguay: Precambrian-Mesozoic Dyke Swarms and Mesozoic Rifting Structural and Tectonic Evolution. *Tectonophysics* **2020**, *789*, 228373. [[CrossRef](#)]
32. Preciozzi, F.; Spoturno, J.; Heinzen, W. Carta Geo-Estructural Del Uruguay a Escala 1/2,000,000. *Inst. Geológico Ing. Eduardo Terra Arocena Montev.* **1979**, *62*, 23.
33. Bossi, J.; Campal, N.; Hartmann, L.A.; Schipilov, A. Predevoniano En El Uruguay: Terrenos y SHRIMP II. In *Actas XI Congreso Latinoamericano de Geología*; Montevideo (CD ROM): Montevideo, Uruguay, 2001.
34. Peel, E.; Bettucci, L.S.; Basei, M.A.S. Geology and Geochronology of Paso Del Dragón Complex (Northeastern Uruguay): Implications on the Evolution of the Dom Feliciano Belt (Western Gondwana). *J. South Am. Earth Sci.* **2018**, *85*, 250–262. [[CrossRef](#)]
35. Morales, E.; Veroslavsky, G.; Manganelli, A.; Marmisolle, J.; Pedro, A.; Samaniego, L.; Plenc, F.; Umpiérrez, R.; Ferreira, M.; Morales, M. Potential of Geothermal Energy in the Onshore Sedimentary Basins of Uruguay. *Geothermics* **2021**, *95*, 102165. [[CrossRef](#)]
36. Rodriguez, P.; Veroslavsky, G.; Soto, M.; Marmisolle, J.; Gristo, P.; Ana, H.D.S. *New Integrated Gravity Bouguer Anomaly Map Onshore Uruguay: Preliminary Implications for the Recognition of Crustal Domains*; SEG New Orleans Annual Meeting: New Orleans, LA, USA, 2015; pp. 1515–1519.
37. Cernuschi, F.; Dilles, J.H.; Kent, A.J.R.; Schroer, G.; Raab, A.K.; Conti, B.; Muzio, R. Geology, Geochemistry and Geochronology of the Cretaceous Lascano East Intrusive Complex and Magmatic Evolution of the Laguna Merín Basin, Uruguay. *Gondwana Res.* **2015**, *28*, 837–857. [[CrossRef](#)]
38. Veroslavsky, G.; Fulfaro, G.; Ana, H.D.S. El Devónico En Uruguay: Estratigrfía, Correlación Geológica y Recursos Minerales. In *Cuencas Sedimentarias de Uruguay: Geología, Paleontología y Recursos Naturales—Paleozoico*; Veroslavsky, G., Ubilla, M., Martínez, S., Eds.; DIRAC—Facultad de Ciencias: Montevideo, Uruguay, 2006; pp. 107–132.
39. Ana, H.D.S.; Goso, C.; Daners, G. Cuenca Norte: Estratigrafía Del Carbonífero–Pérmico. In *Cuencas Sedimentarias de Uruguay: Geología, Paleontología y Recursos Naturales—Paleozoico*; Veroslavsky, G., Ubilla, M., Martínez, S., Eds.; DIRAC—Facultad de Ciencias: Montevideo, Uruguay, 2006; pp. 147–208.
40. Ana, H.D.S.; Veroslavsky, G. La Tectosecuencia Volcanosedimentaria de La Cuenca Norte de Uruguay. Edad Jurásico—Cretácico Temprano. In *Cuencas Sedimentarias de Uruguay: Geología, Paleontología y Recursos Naturales—Mesozoico*; Veroslavsky, G., Ubilla, M., Martínez, S., Eds.; DIRAC—Facultad de Ciencias: Montevideo, Uruguay, 2004; pp. 53–76.
41. Goso, C.; Perea, D. El Cretácico Post-Basáltico y El Terciario Inferior de La Cuenca Litoral Del Río Uruguay: Geología y Paleontología. In *Cuencas Sedimentarias de Uruguay: Geología, Paleontología y Recursos Naturales—Paleozoico*; Veroslavsky, G., Ubilla, M., Martínez, S., Eds.; DIRAC—Facultad de Ciencias: Montevideo, Uruguay, 2004; pp. 143–172.
42. Ucha, N.; De Santa Ana, H. *Evaluación Del Potencial Hidrocarburífero Del Sector Noroccidental de La Cuenca Norte Uruguay*; División Investigación y Desarrollo, ANCAP: Montevideo, Uruguay, 1990.

43. Veroslavsky, G.; Rossello, E.A.; López-Gamundí, O.; Ana, H.D.S.; Assine, M.L.; Marmisolle, J.; Perinotto, A.D.J. Late Paleozoic Tectono-Sedimentary Evolution of Eastern Chaco-Paraná Basin (Uruguay, Brazil, Argentina and Paraguay). *J. South Am. Earth Sci.* **2021**, *106*, 102991. [[CrossRef](#)]
44. Rossello, E.; Ana, H.D.S.; Veroslavsky, G. El Lineamiento Santa Lucía-Aiguá-Merín (Uruguay): Un Corredor Tectónico Extensivo y Transcurrente Dextral Precursor de La Apertura Atlántica. *Rev. Bras. Geociências* **2000**, *30*, 749–756. [[CrossRef](#)]
45. Rossello, E.; Ana, H.D.S.; Veroslavsky, G. *El Lineamiento Santa Lucía-Aiguá-Merín (Uruguay): Un Rifting Transensivo Mesozoico Abortado Durante La Apertura Atlántica. En Anais Do 5º Simpósio Sobre o Cretáceo Do Brasil e 1er Simpósio Sobre o Cretáceo de América Del Sur*; UNSP/SBG: Serra Negra, Brazil, 1999; pp. 443–448.
46. Rossello, E.; Veroslavsky, G.; De Santa Ana, H. Influencias Del Lineamiento Transensivo Santa Lucía-Aiguá-Merín Sobre El Emplazamiento Del Magmatismo Alcalino Cretácico Del Cratón La Plata (Uruguay): Aportes a La Prospección Diamantífera. *Rev. Bras. Geociências* **2001**, *31*, 163–168. [[CrossRef](#)]
47. Ana, H.D.S.; Ucha, N. *Exploration Perspectives and Hydrocarbon Potential of the Uruguayan Sedimentary Basins (Internal Report)*; ANCAP: Manuka, Australia, 1994.
48. Morales, E.; Plenc, F.; Marmisolle, J.; Rossello, E.; Oleaga, A.; Umpiérrez, R. Tectono-Stratigraphic Evolution of the Jurassic-Cretaceous Laguna Merin Basin (Uruguay): New Insights from Magnetotelluric Transects. *Tectonophysics* **2022**, *823*, 229211. [[CrossRef](#)]
49. Turner, S.P.; Peate, D.W.; Hawkesworth, C.J.; Mantovani, M.S.M. Chemical Stratigraphy of the Paraná Basalt Succession in Western Uruguay: Further Evidence for the Diachronous Nature of the Paraná Magma Types. *J. Geodyn.* **1999**, *28*, 459–469. [[CrossRef](#)]
50. Donzé, F.-V.; Truche, L.; Shekari Namin, P.; Lefeuvre, N.; Bazarkina, E.F. Migration of Natural Hydrogen from Deep-Seated Sources in the São Francisco Basin, Brazil. *Geosciences* **2020**, *10*, 346. [[CrossRef](#)]
51. Lefeuvre, N.; Truche, L.; Donzé, F.-V.; Gal, F.; Tremosa, J.; Fakoury, R.-A.; Calassou, S.; Gaucher, E.C. Natural Hydrogen Migration along Thrust Faults in Foothill Basins: The North Pyrenean Frontal Thrust Case Study. *Appl. Geochem.* **2022**, *145*, 105396. [[CrossRef](#)]
52. Roche, V.; Geymond, U.; Boka-Mene, M.; Delcourt, N.; Portier, E.; Revillon, S.; Moretti, I. A New Continental Hydrogen Play in Damara Belt (Namibia). *Sci. Rep.* **2024**, *14*, 11655. [[CrossRef](#)] [[PubMed](#)]
53. Serratt, H.; Cupertino, J.A.; Cruz, M.F.; Girelli, T.J.; Lehn, I.; Teixeira, C.D.; Oliveira, H.O.S.; Chemale Jr, F. Southern Brazil Hydrogen Systems Review. *Int. J. Hydrogen Energy* **2024**, *69*, 347–357. [[CrossRef](#)]
54. Bossi, J.; Schipilov, A. *Rocas Ígneas Básicas Del Uruguay*; Facultad de Agronomía: Montevideo Uruguay, 2000; Volume II.
55. Will, T.M.; Frimmel, H.E.; Gaucher, C.; Bossi, J. Geochemical and Isotopic Composition of Pan-African Metabasalts from Southwestern Gondwana: Evidence of Cretaceous South Atlantic Opening along a Neoproterozoic Back-Arc. *Lithos* **2014**, *202–203*, 363–381. [[CrossRef](#)]
56. Ramos, R.C.; Koester, E. Geología Da Associação Metamáfica-Ultramáfica Da Região de Arroio Grande, Sudeste Do Escudo Sul-Rio-Grandense. *Pesq. Geoc.* **2014**, *41*, 25. [[CrossRef](#)]
57. Gaucher, C.; Frei, R.; Samaniego, L.; Will, T.M.; Chemale, F.; Gargiulo, M.F.; Poiré, D.G.; Ling, X.; Li, X.-H.; Li, Q.-L. The Tapes Complex (Nico Pérez Terrane, Uruguay): Constraining the Mesoproterozoic Evolution of the Río de La Plata Craton. *J. South Am. Earth Sci.* **2021**, *105*, 102906. [[CrossRef](#)]
58. Bossi, J.; Schipilov, A. *Rocas Ígneas Básicas Del Uruguay*; Facultad de Agronomía: Montevideo, Uruguay, 2007; pp. 1–364.
59. Bossi, J.; Ferrando, R. *Carta Geológica Del Uruguay a Escala 1/500,000, Versión Digital 2.0*; Facultad de Agronomía: Montevideo, Uruguay, 2001.
60. Piñeyro, D.; Bossi, J. *Complejo Gabro-Granito Post Orogénico Guaycurú, Uruguay. IV Reunión de Mineralogía y Metalogénia*; Universidad Nacional Del Sur: Bahía Blanca, Argentina, 1998; pp. 301–307.
61. Villar, L.; Segal, S. Caracterización Petrológica y Metalogénica Del Complejo Gábrico Próximo a San José de Mayo, Departamento de San José, Uruguay. *Primer Congr. Urug. Geol.* **1990**, *1*, 199–204.
62. Mari, C.; Costa, H.; Infanzoni, E.; Gonzalez, C.M. *Estudio Geofísico Regional En Sierra de Mahoma, San José*; Actas Del I Congreso Uruguayo de Geología: Montevideo, Uruguay, 1990; Volume 2, pp. 145–150.
63. Schipilov, A.; Iardino, G.; Bossi, J.; Piñeyro, D. *Gabros Hornbléndicos Eoproterozoicos Del Cinturón San José*; Universidad Nacional del Sur: Bahía Blanca, Argentina, 1998.
64. Hartmann, L.A.; Bossi, J.; Santos, J.O.S.; McNaughton, N.; Piñeyro, D. Geocronología U-Pb SHRIMP En Circones Del Gabro Rospide En El Cinturón Paleoproterozoico San José, Terreno Piedra Alta, Uruguay: Una Prueba Geocronológica de Magmas Coetáneos. *Rev. Soc. Urug. Geol.* **2008**, *14*, 40–53.
65. Bossi, J. *Geología Del Uruguay*; Departamento de Publicaciones, Universidad de La República: Montevideo, Uruguay, 1966.
66. Demarco, M.M.; Oyhançabal, P.; Stein, K.-J.; Siegesmund, S. Black Dimensional Stones: Geology, Technical Properties and Deposit Characterization of the Dolerites from Uruguay. *Environ. Earth Sci.* **2011**, *63*, 1879–1909. [[CrossRef](#)]
67. Lossada; Rapolini, A.; Betucci, L.S. Enjambre de Diques Básicos de Nico Pérez—Zapicán, Uruguay: Evidencias Radimétricas y Paleomagnéticas Sobre Su Edad. *Rev. Asoc. Geológica Argent.* **2014**, *71*, 345–355.

68. Oriolo, S.; Oyhantçabal, P.; Basei, M.A.S.; Wemmer, K.; Siegesmund, S. The Nico Pérez Terrane (Uruguay): From Archean Crustal Growth and Connections with the Congo Craton to Late Neoproterozoic Accretion to the Río de La Plata Craton. *Precambrian Res.* **2016**, *280*, 147–160. [[CrossRef](#)]
69. Santos, J.O.S.; Hartmann, L.A.; Bossi, J.; Campal, N.; Schipilov, A.; Piñeyro, D.; McNaughton, N.J. Duration of the Trans-Amazonian Cycle and Its Correlation within South America Based on U-Pb SHRIMP Geochronology of the La Plata Craton, Uruguay. *Int. Geol. Rev.* **2003**, *45*, 27–48. [[CrossRef](#)]
70. Bossi, J.; Gaucher, C. Formación Valentines. *Geol. Urug.* **2014**, *1*, 171–189.
71. Lancaster, H. Mineralogy, Geochemistry, and Genesis of the Valentines Iron Formation, Nico Pérez Terrane, Eastern Uruguay, and Significance for the Redox Conditions of Early Earth's Oceans. Master's Thesis, East Carolina University, Greenville, NC, USA, 2015.
72. Rosière, C.A.; Heimann, A.; Oyhantçabal, P.; Santos, J.O.S. The Iron Formations of the South American Platform. In *Geology of Southwest Gondwana*; Siegesmund, S., Basei, M.A.S., Oyhantçabal, P., Oriolo, S., Eds.; Regional Geology Reviews; Springer International Publishing: Cham, Switzerland, 2018; pp. 493–526. ISBN 978-3-319-68919-7.
73. Oyhantçabal, P.; Wagner-Eimer, M.; Wemmer, K.; Schulz, B.; Frei, R.; Siegesmund, S. Paleo- and Neoproterozoic Magmatic and Tectonometamorphic Evolution of the Isla Cristalina de Rivera (Nico Pérez Terrane, Uruguay). *Int. J. Earth Sci.* **2012**, *101*, 1745–1762. [[CrossRef](#)]
74. Oyhantçabal, P.; Oriolo, S.; Wemmer, K.; Basei, M.A.S.; Frei, D.; Siegesmund, S. Provenance of Metasedimentary Rocks of the Western Dom Feliciano Belt in Uruguay: Insights from U–Pb Detrital Zircon Geochronology, Hf and Nd Model Ages, and Geochemical Data. *J. South Am. Earth Sci.* **2021**, *108*, 103139. [[CrossRef](#)]
75. Hartmann, L.A.; Campal, N.; Santos, J.O.S.; McNaughton, N.J.; Bossi, J.; Schipilov, A.; Lafon, J.-M. Archean Crust in the Rio de La Plata Craton, Uruguay—SHRIMP U–Pb Zircon Reconnaissance Geochronology. *J. South Am. Earth Sci.* **2001**, *14*, 557–570. [[CrossRef](#)]
76. Gaucher, C. Integrated Correlation of the Vendian to Cambrian Arroyo Del Soldado and Corumbá Groups (Uruguay and Brazil): Palaeogeographic, Palaeoclimatic and Palaeobiologic Implications. *Precambrian Res.* **2003**, *120*, 241–278. [[CrossRef](#)]
77. Gaucher, C.; Sial, A.N.; Blanco, G.; Sprechmann, P. Chemostratigraphy of the Lower Arroyo Del Soldado Group (Vendian, Uruguay) and Palaeoclimatic Implications. *Gondwana Res.* **2004**, *7*, 715–730. [[CrossRef](#)]
78. Cabrera, J.; Gaucher, C.; Frei, R.; Sial, A.N.; Ferreira, V.P. Formación Manguera Azul. *Geol. Urug.* **2014**, *1*, 191–208.
79. Oriolo, S.; Oyhantçabal, P.; Konopásek, J.; Basei, M.A.S.; Frei, R.; Sláma, J.; Wemmer, K.; Siegesmund, S. Late Paleoproterozoic and Mesoproterozoic Magmatism of the Nico Pérez Terrane (Uruguay): Tightening up Correlations in Southwestern Gondwana. *Precambrian Res.* **2019**, *327*, 296–313. [[CrossRef](#)]
80. Spoturno, J.; Oyhantçabal, P.; Loureiro, J. *Mapa Geológico Del Departamento de Maldonado a Escala 1:100,000, Cap. 2 Geología*; Facultad de Ciencias (UdelaR)—Dirección Nacional de Minería y Geología (MIEM): Montevideo, Uruguay, 2012.
81. Preciozzi, F.; Spoturno, J.; Heinzen, W.; Rossi, P. *Carta Geologica Del Uruguay a Escala 1:500000, Texto Explicativo*; Ministerio Industria Energia: Montevideo, Uruguay, 1985.
82. Hartmann, L.A.; Santos, J.O.S.; Bossi, J.; Campal, N.; Schipilov, A.; McNaughton, N.J. Zircon and Titanite U–Pb SHRIMP Geochronology of Neoproterozoic Felsic Magmatism on the Eastern Border of the Rio de La Plata Craton, Uruguay. *J. South Am. Earth Sci.* **2002**, *15*, 229–236. [[CrossRef](#)]
83. Gaucher, C.; Bossi, J.; Frei, R.; Remus, M.; Piñeyro, D. Terreno Cuchilla Dionisio: Bloque Septentrional. *Geol. Urug.* **2014**, *1*, 377–400.
84. Oyhantçabal, P.; Siegesmund, S.; Wemmer, K.; Frei, R.; Layer, P. Post-Collisional Transition from Calc-Alkaline to Alkaline Magmatism during Transcurrent Deformation in the Southernmost Dom Feliciano Belt (Braziliano–Pan-African, Uruguay). *Lithos* **2007**, *98*, 141–159. [[CrossRef](#)]
85. De Santa Ana, H.; Conti, B.; Ferro, S.; Gristo, P.; Marmisolle, J.; Rodriguez, P.; Soto, M.; Tomasini, J. Estado Actual de Los Hidrocarburos y Otros Recursos Energéticos En Uruguay. *Petrotecnia* **2010**, *51*, 30–40.
86. Conti, B.; Gristo, P.; Torres, M.; Castiglioni, J.; Patrice, P.; Morales Demarco, M.; Yermán, L. Characterization of Permian Mangrullo Formation (Uruguay) Oil Shale as a Source Rock and Its Correlation with Iratí (Brazil) and Whitehill (South Africa) Formations. In Proceedings of the International Conference and Exhibition, Cape Town, South Africa, 4–7 November 2019.
87. Torres, M.; Castiglioni, J.; Yermán, L.; Suescun, L.; Conti, B.; Demarco, M.M.; Gristo, P.; Portugau, P.; Cuña, A. Assessment of Uruguayan Oil Shales: Physicochemical, Thermal and Morphological Characterization. *Fuel* **2018**, *234*, 347–357. [[CrossRef](#)]
88. Marmisolle, J. Análisis Tectonosedimentario de Depocentros En El Sector Noroeste de Cuenca Norte. Master's Thesis, PEDECIBA, Montevideo, Uruguay, 2015.
89. Peel, E.; Muzio, R.; Fort, S.; Olivera, L. Precambrian Basement Rocks of the Southernmost Tip of the Paraná Basin (Northern Uruguay): Petrologic Assessment from Deep Borehole Data. *Precambrian Res.* **2024**, *404*, 107323. [[CrossRef](#)]
90. Coveney, R.M.; Goebel, E.D.; Zeller, E.; Dreschhoff, G. Serpentinization and the Origin of Hydrogen Gas in Kansas. *Bulletin* **1987**, *71*, 39–48. [[CrossRef](#)]

91. McCollom, T.M.; Bach, W. Thermodynamic Constraints on Hydrogen Generation during Serpentinization of Ultramafic Rocks. *Geochim. Cosmochim. Acta* **2009**, *73*, 856–875. [[CrossRef](#)]
92. Morales, E.; Pedro, A.; De León, R. Geothermal Gradients and Heat Flow in Norte Basin of Uruguay. *Int. J. Terr. Heat Flow Appl.* **2020**, *3*, 20–25. [[CrossRef](#)]
93. De León, R.; Morales, E.; PintoVieira, F. Thermal Regime of the Northwestern Sector of the Norte Basin (Uruguay): Geothermal Gradient and Heat Flow. *J. South Am. Earth Sci.* **2022**, *116*, 103862. [[CrossRef](#)]
94. Leong, J.A.; Nielsen, M.; McQueen, N.; Karolytè, R.; Hillemonds, D.J.; Ballentine, C.; Darrah, T.; McGillis, W.; Kelemen, P. H₂ and CH₄ Outgassing Rates in the Samail Ophiolite, Oman: Implications for Low-Temperature, Continental Serpentinization Rates. *Geochim. Cosmochim. Acta* **2023**, *347*, 1–15. [[CrossRef](#)]
95. Geymond, U.; Briollet, T.; Combaudon, V.; Sissmann, O.; Martinez, I.; Duttine, M.; Moretti, I. Reassessing the Role of Magnetite during Natural Hydrogen Generation. *Front. Earth Sci.* **2023**, *11*, 1169356. [[CrossRef](#)]
96. Milesi, V.; Guyot, F.; Brunet, F.; Richard, L.; Recham, N.; Benedetti, M.; Dairou, J.; Prinzhofer, A. Formation of CO₂, H₂ and Condensed Carbon from Siderite Dissolution in the 200–300 °C Range and at 50 MPa. *Geochim. Cosmochim. Acta* **2015**, *154*, 201–211. [[CrossRef](#)]
97. Gemeiner, H.; Teramoto, E.H.; Veroslavsky, G.; Chang, H.K. Using Dissolved Noble Gases to Characterize the Groundwaters of the Southern Portion of the Guarani Aquifer System at the Brazil-Uruguay Border Region. 2024. Available online: https://papers.ssrn.com/sol3/papers.cfm?abstract_id=4992909 (accessed on 22 January 2025).
98. Horsfield, B.; Mahlstedt, N.; Weniger, P.; Misch, D.; Vranjes-Wessely, S.; Han, S.; Wang, C. Molecular Hydrogen from Organic Sources in the Deep Songliao Basin, P.R. China. *Int. J. Hydrogen Energy* **2022**, *47*, 16750–16774. [[CrossRef](#)]
99. Moretti, I.; Bouton, N.; Ammouial, J.; Ramirez, A.C. The H₂ Potential of the Colombian Coals in Natural Conditions. *Int. J. Hydrogen Energy* **2024**, *77*, 1443–1456. [[CrossRef](#)]
100. Maiga, O.; Deville, E.; Laval, J.; Prinzhofer, A.; Diallo, A.B. Trapping Processes of Large Volumes of Natural Hydrogen in the Subsurface: The Emblematic Case of the Bourakebougou H₂ Field in Mali. *Int. J. Hydrogen Energy* **2024**, *50*, 640–647. [[CrossRef](#)]
101. Soto, M. Geología, Geofísica y Geoquímica de La Región de Pepe Núñez, Cuenca Norte (Uruguay). Master's Thesis, PEDECIBA, Montevideo, Uruguay, 2014.
102. Geymond, U.; Ramanaidou, E.; Lévy, D.; Ouaya, A.; Moretti, I. Can Weathering of Banded Iron Formations Generate Natural Hydrogen? Evidence from Australia, Brazil and South Africa. *Minerals* **2022**, *12*, 163. [[CrossRef](#)]
103. Veroslavsky, G.; Rossello, E.; De Santa Ana, H. La Anomalía Gravimétrica de La Laguna Merín: Origen y Expectativas En La Exploración Mineral. *Rev. Soc. Urug. Geol.* **2002**, *1*, 21–28.
104. De Santa Ana, H. *Análise Tectono-Estratigráfica Das Sequências Permotriássica e Jurocretácea Da Bacia Chacoparanense Uruguaia (“Cuenca Norte”)*; Universidade Estadual Paulista (Unesp): São Paulo, Brazil, 2004.
105. Baranenko, V.I.; Kirov, V.S. Solubility of Hydrogen in Water in a Broad Temperature and Pressure Range. *At. Energy* **1989**, *66*, 30–34. [[CrossRef](#)]
106. Lopez-Lazaro, C.; Bachaud, P.; Moretti, I.; Ferrando, N. Predicting the Phase Behavior of Hydrogen in NaCl Brines by Molecular Simulation for Geological Applications. *BSGF—Earth Sci. Bull.* **2019**, *190*, 7. [[CrossRef](#)]
107. Olivares, C.; Findlay, J.; Kelly, R.; Otto, S.; Norman, M.; Cairns, M. A New Exploration Tool in the Search for Native Hydrogen and Helium. *Geol. Soc. London Spéc. Publ.* **2024**, *547*, 527–534. [[CrossRef](#)]
108. França, A.B. Glacial-Related Sandstones of the Gondwanan Itarare Group (CP), and the Barra Bonita Gas Field, Parana Basin, Brazil. In Proceedings of the AAPG International Conference and Exhibition, Perth, Australia, 5–8 November 2006.
109. Ren, K.; Zhao, J.; Liu, Q.; Zhao, J. Hydrocarbons in Igneous Rock of Brazil: A Review. *Pet. Res.* **2020**, *5*, 265–275. [[CrossRef](#)]

Disclaimer/Publisher's Note: The statements, opinions and data contained in all publications are solely those of the individual author(s) and contributor(s) and not of MDPI and/or the editor(s). MDPI and/or the editor(s) disclaim responsibility for any injury to people or property resulting from any ideas, methods, instructions or products referred to in the content.